ANKARA YILDIRIM BEYAZIT UNIVERSITY
GRADUATE SCHOOL OF NATURAL AND APPLIED SCIENCES

CONTROL AND COMPARISON OF AN ELECTROMECHANICALLY ACTUATED CONTROL SURFACE ACCORDING TO DIFFERENT SENSOR LOCATIONS

M.Sc. Thesis by

Ömer KOÇ

Department of Defence Technologies

January, 2021

ANKARA

CONTROL AND COMPARISON OF AN ELECTROMECHANICALLY ACTUATED CONTROL SURFACE ACCORDING TO DIFFERENT SENSOR LOCATIONS

A Thesis Submitted to

The Graduate School of Natural and Applied Sciences of Yıldırım Beyazıt University

In Partial Fulfillment of the Requirements for the Degree of Master of Science in Defence Technologies, Department of Defence Technologies

by

Ömer KOÇ

January, 2021

ANKARA

M.Sc. THESIS EXAMINATION RESULT FORM

We have read the thesis entitled "**CONTROL AND COMPARISON OF AN ELECTROMECHANICALLY ACTUATED CONTROL SURFACE ACCORDING TO DIFFERENT SENSOR LOCATIONS**" completed by **ÖMER KOÇ** under supervision of **PROF. DR. HÜSEYİN CANBOLAT** and we certify that in our opinion it is fully adequate, in scope and in quality, as a thesis for the degree of Master of Science.

Prof. Dr. Hüseyin CANBOLAT

Supervisor

Prof. Dr. Arif ANKARALI

Jury Member

Dr. Öğr. Üyesi Hakan TORA

Jury Member

Prof. Dr. Ergün ERASLAN

Director

Graduate School of Natural and Applied Sciences

ETHICAL DECLARATION FORM

I hereby declare that, in this thesis which has been prepared in accordance with the Thesis Writing Manual of Graduate School of Natural and Applied Sciences,

- All data, information and documents are obtained in the framework of academic and ethical rules,
- All information, documents and assessments are presented in accordance with scientific ethics and morals,
- All the materials that have been utilized are fully cited and referenced,
- No change has been made on the utilized materials,
- All the works presented are original, and in any contrary case of above statements, I accept to renounce all my legal rights

Date: **Signature:…………………………**

Name & Surname: Ömer KOÇ

ACKNOWLEDGMENTS

I would like to take this opportunity to thank my supervisor, Prof. Dr. Hüseyin CANBOLAT, for his guidance, moral support and advices. Thanks for his great contribution on this work that I could complete my thesis.

I also wish to thank Yasin YENİAYDIN, Dr. Ersin DAŞ and Berkay BAYKARA for their great support and advices.

I also wish to thank TÜBİTAK SAGE; this work was supported from the initial stages to the end.

Finally, I am very thankful to my wife Zeynep KOÇ.

Ömer KOÇ

CONTROL AND COMPARISON OF AN ELECTROMECHANICALLY ACTUATED CONTROL SURFACE ACCORDING TO DIFFERENT SENSOR LOCATIONS

ABSTRACT

In missile systems with a control actuation system, in terms of control methods, sensors and their locations have an important effect on control methods. Transmission mechanisms between the sensor measuring locations and control surfaces make control of system difficult due to their non-linear behavior. This nonlinear situation is caused by backlash and deformations between control surfaces and sensor position. In this study, differences between direct feedback and indirect feedback and differences caused by these differences in terms of controller will be examined. In order to study this situation, position sensors are placed on two different mechanism parts for an electromechanical fin actuation system, which is responsible for directing a missile. After this placement, system identification of the fin actuation system has been made with measurement from fin angle. After that, controllers have been designed. The first controller was designed by method of state feedback. In first simulation studies, it is observed that the controller made steady state errors under the disturbing effect. In order to eliminate the steady state error, an integrally effective outer loop has been added to the controller that the error resets. As an alternative to the controller designed with state feedback method, a PID controller with same roots has been designed. Then the controllers are in real time tested. In order to minimize the effects of measurement errors and nonlinearities, backlash and material deformations caused by the nature of the mechanism by using the feedback from two different sensors, it has been observed that the system response is cleared from the error values caused by the backlash and the system can be controlled more accurately.

Keywords: Electromechanical, Sensor, Control

ELEKTROMEKANİK EYLETİMLİ BİR KONTROL YÜZEYİNİN FARKLI ALGILAYICI YERLEŞİMİNE GÖRE DENETİMİ VE KARŞILAŞTIRILMASI

ÖZ

Kontrol tahrik sistemine sahip olan mühimmatlarda algılayıcılar ve bu algılayıların yerleşim yerleri kontrol yöntemleri açısından önemli bir girdiye sahiptir. Algılayıcı ölçüm yerleri ile kontrol yüzeyleri arasındaki aktarma mekanizmalarının doğrusal olmayan davranışlarından dolayı sistemin kontrolünü güçleştirmektedir. Bu doğrusal olmayan durum mekanizmanın ve kontrol yüzeyi ile algılayıcı konumu arasındaki mekanik boşluk ve esnemelerden kaynaklanmaktadır. Bu çalışmada doğrudan geribesleme ve dolaylı geri besleme arasındaki farklar ve bu farkların kontrolcü açısından oluşturduğu farklılıklar incelenecektir. Bunun için bir mühimmatın yönlendirilmesinde görevli elektromekanik kanatçık tahrik sistemi için iki farklı mekanizma uzvuna açı(konum) algılayıcı yerleşimi yapılmıştır. Bu yerleşim sonrasında tahrik sisteminin sistem tanımlaması kanatçıktan ölçülen algılayıcıdan alınan veri ile yapılmıştır. Daha sonrasında denetleyicilerin tasarım aşamasına geçilmiştir. Tasarlanan ilk denetleyici durum uzayı geribesleme yöntemi ile yapılmıştır. Yapılan ilk benzetim çalışmalarında denetleyicinin bozucu etki altında kalıcı durum hatasına neden olduğu gözlemlenmiştir. Kalıcı durum hatasının giderilmesi amacı ile denetleyiciye integral etkili bir dış döngü eklenmiş ve hatanın sıfırlandığı görülmüştür. Durum geribesleme yöntemi ile tasarlanan kontrolcüye alternatif olarak aynı köklere sahip olacak şekilde bir PID (Oransal-İntegral-Türevsel) denetleyici tasarlanmıştır. Daha sonra gerçek zamanlı olarak test edilmiştir. Mekanizmanın doğası gereği oluşan açı sapmaları, boşlukların ve deformasyonların etkilerini en aza indirgemek ve doğrusal olmayan etkileri denetleyicide görmemek için iki farklı algılayıcıdan alınan geri besleme ile birlikte kullanılarak sistem cevabının, boşlukların oluşturduğu hata değerlerinden arındırıldığı ve sistemin daha doğru kontrol edilebileceği gösterilmiştir.

Anahtar Kelimeler: Elektromekanik, Kontrol, Algılayıcı

CONTENTS

LIST OF ABBREVIATIONS AND SYMBOLS

ARMAX	Auto Regression with Moving Average and Extra Input
ARX	Autoregressive Models with Exogenous Variables
BJ	Box Jenkins
CCF	Cross-Correlation Function
DC	Direct Current
EMC	Electromagnetic Compatibility
FAS	Fin Actuation System
I/O	Input/Output
OE	Output Error
PID	Proportional, Integral, Derivative
PRBS	Pseudo Random Binary Sequence
RMS	Root Mean Square
rpm	Revolutions Per Minute
VAF	Variance Accounted For
$\ddot{\theta}_F$	Angular Acceleration of the Fin
$\dot{\theta}_F$	Angular Velocity of the Fin
$\dot{\theta}_M$	Angular Velocity of the DC motor
ω_n	Natural Frequency
B_F	Viscous Friction Constant
$C_{DISCRETE\_PID}$	Transfer Function of Discrete-Time PID Controller
C_{PID}	Transfer Function of the PID Controller
G_{CL}	Transfer Function of the Closed-Loop System
G_{plant}	Transfer Function of the Plant
J_F	Moment of Inertia of the System According to Fin Axis
J_{link}	Moment of Inertia of the Moment Arm
J_{motor}	Moment of Inertia of the DC Motor
J_{shaft}	Moment of Inertia of the DC Motor Shaft
K_P, K_I, K_D	Proportional Gain, Integral Gain, Derivative Gain
K_t	Torque Constant of DC Motor
L_{link}	Length of the Moment Arm
$\tilde{N}$	Additive Gain
S_{C1}	Controllability Matrix of State Space System without Integral Action
S_{C2}	Controllability Matrix of State Space System with Integral Action
S_{O1}	Observability Matrix of State Space System without Integral Action
S_{O2}	Observability Matrix of State Space System with Integral Action
a_1	Distance between Two Axes
a_2	Moment Arm Length
k_1	First Term of Controller Matrix
k_2	Second Term of Controller Matrix
$m_{equivalent}$	Equivalent Mass
m_{nut}	Mass of the Ballscrew-Nut
v_{nut}	Velocity of the Ballscrew-Nut
$\dot{x}$	Time Derivative of Vector x
$\hat{y}$	Estimated Data

θ_{12}	Fin Angle
θ_{14}	Misalignment Angle
A	Ampere
H	Gain
Hz	Hertz
Nm	Newton Meter
ξ	Damping Ratio
A	State Matrix
B	Input Matrix
C	Output Matrix
D	Feedthrough Matrix
K	Controller Matrix
N	Fixed Transmission Ratio of the System (According to the Velocities)
Re	Real Part of a Complex Number
Ruu	Autocorrelation Function of the Input u
Ruy	Cross-Correlation Function between Input u and Output y
c	Misalignment
g	Weight Sequence
i	Current
n	White Noise Signal
r	Reference
s	Displacement of Ballscrew-Nut
u	Input Vector
x	State Vector
y	Output Vector
σ	Step Signal

LIST OF TABLES

LIST OF FIGURES

CHAPTER 1

INTRODUCTION

The Actuation systems used in missiles are diverse. One of these actuation types is the electromechanical fin actuation system. In these systems, the fin angle commands from the guidance control unit of the missile are generally fulfilled by an electric motor and transmission mechanism. In order to verify that this order has been fulfilled, a measurement must be taken from a part of the FAS mechanism with a sensor for feedback. Since transmission mechanisms are generally used in FAS, backlash and deformations in the transmission mechanism in the feedback received by the motor cause some error in the system output angle. In their work in [1], they used the angle at the output shaft (after the transmission elements) of a FAS mechanism as feedback. In reference [2], before the transmission elements in the mechanism, it is used as direct feedback of the motor angle.

In this study, inverted slider-crank mechanisms are used as FAS speed and power transmission mechanism. The torques, which are produced by the electric motors, in the limited volume within the missile are often not sufficient to control the missiles. Motors, which are at a sufficient level, cannot be used at the desired location due to their large volume. For this, motor output torques are generally increased by a transmission mechanism. Examples of these mechanisms are gear, inverted slider-crank, cam mechanisms. In the studies in [3], the kinematic and dynamic analyzes of the inverted slider-crank mechanism have been examined, and the structural features have been scientifically revealed with the real-time fin loading test system. For the FAS, whose design phase has been completed, to be used in the simulation environment, the system must be converted into a mathematical model that can be represented in a simulation environment. This process is called system identification. System identification means obtaining the dynamic model and model parameters of the system by using experimental data [4].

Different methods have been used for the FAS controller design. These are PID(Proportional, Integral, Derivative), Robust, Sliding Mode and State Space controller methods in reference [2], the Robust control method was applied on the FAS and in reference [5], a direct current motor was driven with PID and Sliding Mode control methods. In reference [6], the state feedback controller method has been applied to servo motors.

In this study, it is observed that the controller designed with the pole placement method is not resistant to disturbing effects, and the improved controller obtained by adding a pole to the closed-loop system, which has an integral effect, is found to be resistant to disturbing effects. As a result of the controller studies, the performance of the system and the controller could be verified by applying a disruptive effect from the outside via the Fin Loading System. In this study, unlike the literature, a controller is designed by minimizing the disadvantages of two separate located sensors. Simulations are done by using MATLAB® -SIMULINK®, real-time tests are done by using MATLAB® -xPC Target®.

CHAPTER 2

SYSTEM OVERVIEW

In general, missiles consist of guidance control, warhead, propulsion system, and motion control systems. Some missiles also have a seeker head. To guide the missile to the target, the missile can be controlled from various surfaces. The most common of these is the fin actuation system. General missile structure could be seen in Figure 2.1.

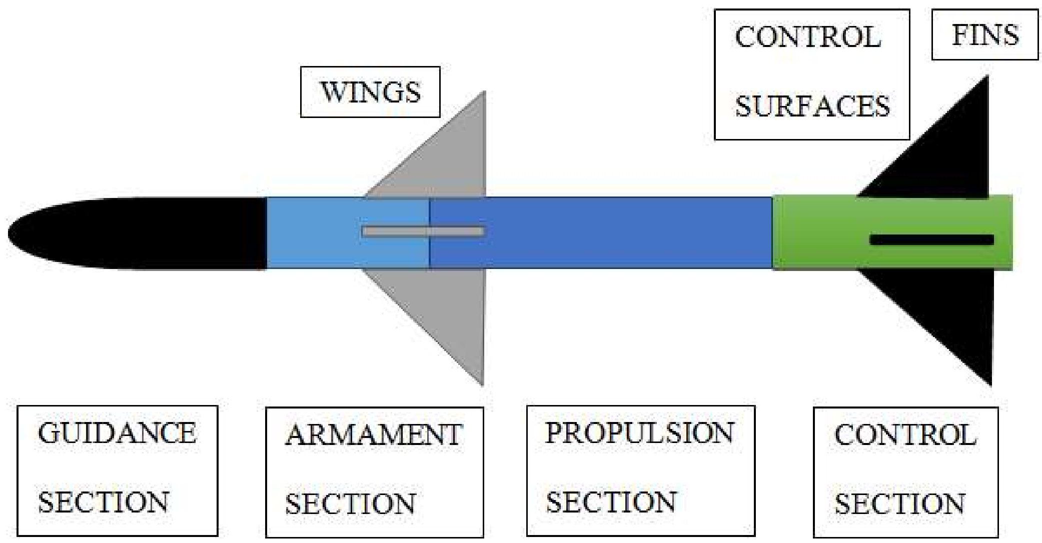

Figure 2.1 General missile structure

2.1 Mechanical Structure

In our system, we use to rotate fin an inverted slider-crank mechanism as an example of 4-link mechanisms. In Figure 2.2 an inverted slider-crank mechanism could be seen. The servo motor, which is connected to the body with a joint, rotates the ball screw. The ball screw converts the rotational motion to the linear motion. The body, which has a length, a_2 rotates because of the linear motion of the ball screw nut.

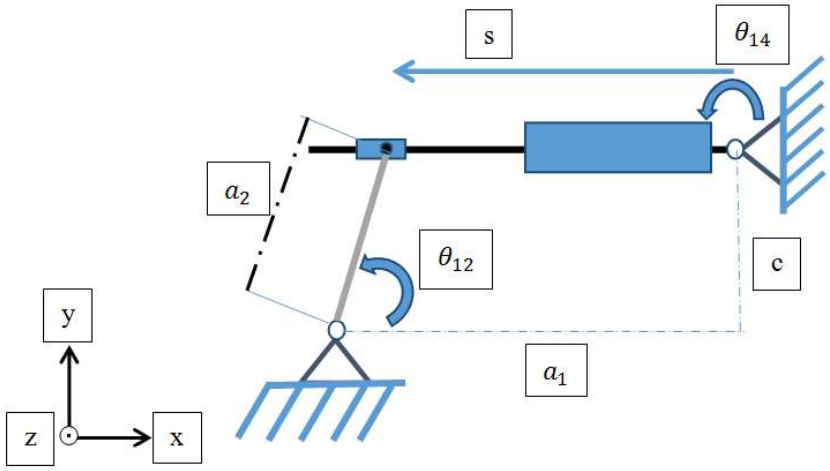

Figure 2.2 Inverted slider crank mechanism

2.2 Feedback Sensor

The sensor is a critical part of the system. Because of this selection of sensors is important. To make a good selection, the sensor has to fulfill the necessity of the system. Geometrical size is important because the sensor has to fit in a designed volume. Resolution and accuracy are other important issues. The encoder, which is used in the system, is a hall-effect magnetic encoder. It has a 10-bit resolution. This is located both on the motor and load side. Because of the fin axis angle measurement, there is no estimation requirement. But the resolution of the encoder is limited. Therefore for better reference tracking both sensors in two different locations could be used. With these sensor locations, the effects of backlash could be compensated. A hall-effect magnetic encoder is shown in Figure 2.3.

The Hall-effect sensor arrangement consists of a plate with only one magnetized pole pair. The plate is attached to the rotor of the sensor and thereby coupled to the rotor movement to be measured. A microprocessor detects the change in direction of the magnetic field when the plate (or rotor) rotates above the microprocessor. These changes in the magnetic field are converted into an analog signal proportional to the change in the angle of the rotating plate. The advantages of such simple sensors include their very compact design, high reliability and linearity, and low susceptibility to electromagnetic compatibility (EMC) interference. The sensors must offer very good protection against environmental influences, reliable storage of the moving parts, good mounting options, and high resistance to mechanical influences.

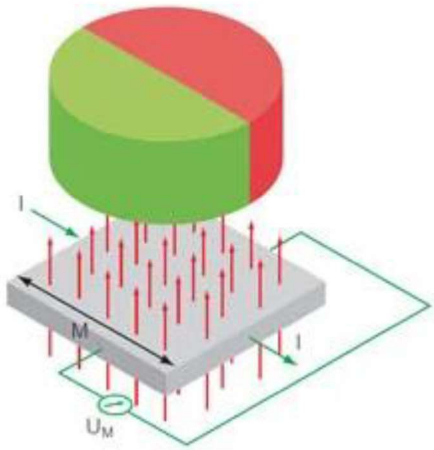

Figure 2.3 Hall-effect magnetic encoder [7]

2.3 Brushless DC Motor

Mainly, the structure of a brushless DC motor consists of a stator and a rotor. The stator forms the outer part of the motor and is made up of at least three coils with iron cores. The rotor sits in the middle of the motor and consists of at least one permanent magnet.

If coils of the stator are a power source connected, each one generates its own magnetic field. By superimposing the individual fields, a total field is created in the middle of the motor. The more coils are attached to the motor, and the smaller the distance between the coils is, the more homogeneous the magnetic field, and the more the rotational movement becomes more stable. In Figure 2.4 is shown a brushless dc motor.

The coils are fed with a sinusoidal current, each is by 120 degrees out of phase, results from the fact that the entire field rotates at a constant speed.

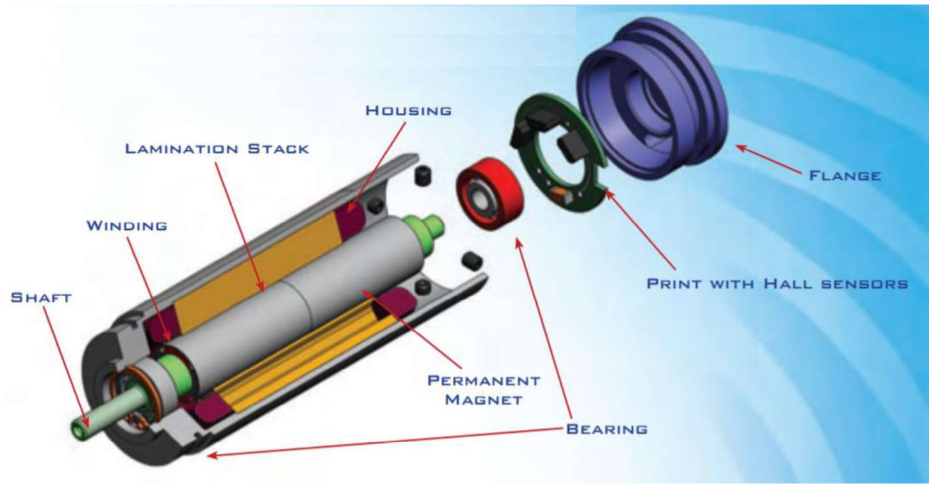

Figure 2.4 A brushless DC motor with bearing components [8]

This so-called rotating field thus continuously changes its orientation and pulls the magnetic field generated by the permanent magnet of the rotor the magnetic transverse pressure with. Thus the rotor follows the rotation of the rotating field and the motor moves [9].

The choice between a brushless and a brushed DC motor has far-reaching consequences and should be subject to the requirements profile of the application concerned, as the performance characteristics of the two designs differ significantly. Factors such as acquisition and maintenance costs must also be taken into account.

The effects and differences of brushed and brushless commutation systems must be taken into account, particularly with a view to the service life of the DC motor. Because of sliding contacts or brushes, mechanically working components, there is continuous abrasion; the useful life is limited. High speeds, vibrations, and similar factors represent additional stress and can have a major impact on the service life of the brushes. The service life of brushless DC motors, on the other hand, is only limited by the built-in ball bearings and can be calculated as realistic as possible. The lack of mechanical friction avoids the risk of brush fire and sparks on the commutator. Brushes also limit their use under specific environmental conditions; for example, only brushless DC motors can be used for high vacuum applications.

In direct comparison with brush motors, brushless DC motors have various performance advantages. These can vary depending on the application and be manifold, but they usually include a higher starting torque, extremely precise - and load fluctuations concerning more resistant - control as well as higher speeds.

In this study, a brushless DC Motor is used because of its high speed and performance. The characteristics of dc motor could be seen in Table 1.1

Table 1.1 Characteristics of DC motor

No load speed	5000 rpm
Torque constant(K_t)	0.1 Nm/A
Moment of inertia	$1.5520 \cdot 10^{-5}$ kgm^2

CHAPTER 3

SYSTEM IDENTIFICATION

The language of technology is mathematics, which enables a compact description of parts of reality with a high degree of standardization. If part of the reality wanted to be described by using a set of equations and if statements about the reality with the interpretation of the mathematical properties wanted to be made, it is spoken of a model. But how can be obtained the appropriate mathematical description from a selected part of reality? One possibility is theoretical modeling, in which the knowledge of elementary internal connections leads to a system of equations that can ultimately be analytically simplified and standardized. In contrast, there is experimental modeling or identification, which only obtains a mathematical model in standard form from the measurement of input signals and assigned output signals. However, many structural assumptions are necessary (e.g. linearity), which more or less limit the applicability. The phenomenon of measurement noise, which must not be ignored, is particularly important.

The latter type is also called black-box models because nothing is known about the internal structure from the start and it has to be made assumptions about the structure. The parameters of the model are then estimated using a suitable algorithm.

Really important is the validation of the model, which means checking whether the model actually matches the reality. This important component of identification must be carefully considered from the outset, as a model is never better than its validation.

The model in the form of a mathematical description is also suitable for experiments in the form of a numerical simulation on the computer. Depending on the computing power, questions can be answered much more quickly and limits can be examined without risk.

There are also pitfalls in model building and simulation: A model that is too simple does not reflect all aspects of the real process, while a model that is too complex requires a lot of time and effort in the creation and simulation. After all, a model can also be simply wrong due to poor or unsuitable structural assumptions. The Figure 3.1 illustrates step of the system identification.

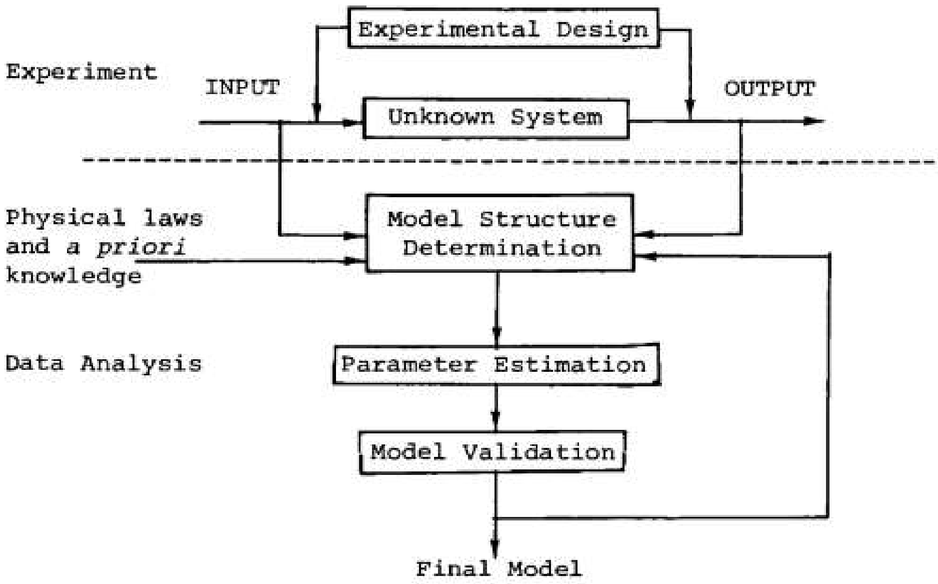

Figure 3.1 Steps of system identification [10]

3.1 Step Response

According to the definition of the step response, a step-shaped input $u(t) = \sigma(t)$ is given to the system. The resulting output is then viewed as a non-parametric model of the system.

The following information can be obtained from considering the step response:

- The outputs (variables) affected by the specific input can be determined.
- The time constants of the system are clearly visible.
- The characteristics (amplification, vibratory, weakly damped, aperiodic, with dead time) of the system become clear.

Because of the simple implementation and immediate information, this method is still very common in the industry. However, there are also disadvantages associated with this:

- Limitations in the input amplitude together with measurement errors and noise impair the accuracy of the result considerably.
- The result is only suitable for a simulation to a limited extent (using a finite convolution sum).

In order to avoid the second point, methods are developed that read a parametric model from the step response. Since these procedures are already relatively old, continuous models are determined from continuous functional processes [11].

3.2 PRBS (Pseudo Random Binary Sequence)

According to reference [12] the PRBS is explained as follows:

> A PRBS signal is a popular input signal for system identification because it is persistently exciting to the order of the period of the signal. A PRBS signal is a series of step functions generated by a series of shift registers with an exclusive or operator [13]. A maximum length PRBS signal has a correlation function that resembles a white noise correlation function. This property does not hold for non-maximum length sequences. The maximum possible period for a maximum length sequence is $\mu = 2\eta - 1$ where η is the order of the PRBS. Thus the PRBS signal used in identification processes should be a maximum length PRBS signal.

3.3 Model Validation

During model validation, the prediction error of the individual models is typically compared with one another. However, the following must be observed:

If it is a sufficiently high model order despite the wrong model structure chosen, then the model is able to provide a good prediction for the training data. However, it could be calculated as a prediction for validation data that is not used in training. In general, the prediction error for the training data decreases continuously with the model order, while the prediction error for the validation data has a minimum with the correct model order.

3.4 Correlation Analysis

The correlation analysis enables a quick insight into time constants and delays (dead times) with simple means.

Advantages and disadvantages of the process are:

- A quick insight into the system dynamics.
- No special input signals are required, measurement noise can be compensated for by signal length.
- The measurement noise does not have to meet any special conditions (only mean value-free with input uncorrelated).
- The result (weight function) cannot be used directly for the simulation.
- In the closed control loop, if the measurement noise is correlated with the input and the method delivers incorrect results [14].

The starting point of the procedure is the so-called Wiener-Hopf equation:

$$R_{uy}(\tau) = \sum_{k=0}^{\infty} g(k)\, R_{uu}(k+\tau) \qquad \mathbf{(3.1)}$$

where R_{uy} is the cross-correlation function between input$u$and output$y$, R_{uu} is the autocorrelation function of the input signal and g is the weight sequence of a discrete system.

In the special case of white noise as input, however, applies to the autocorrelation function of the input

$$R_{uu}(\tau) = \begin{cases} \lambda, & \tau = 0 \\ 0, & \tau \neq 0 \end{cases} \qquad \mathbf{(3.2)}$$

which simplifies the equation 3.1 to

$$R_{uy}(\tau) = \lambda g(\tau) \qquad \mathbf{(3.3)}$$

Equation states that in the case of white noise as input, the function between input and output is equal to the weight sequence g.

In the practical application, two extensions have to be made:

1. The actual CCF is unknown; it must therefore be replaced by an estimate.

$$R_{uy} = \frac{1}{N-\tau}\sum_{k=1}^{N-\tau} u(k)\, y(\tau - k) \tag{3.4}$$

Matlab performs this calculation using the $xcorr$ command with the 'unbiased' option.

2. Since the real input signal is usually not a white noise signal, the measured signals u and y must be filtered with a filter F; The filtered input signal should be as similar as possible to the white noise signal. Then one can estimate the weight sequence g with the filtered signals as described above. Block diagram of the filter could be seen in Figure 3.2.

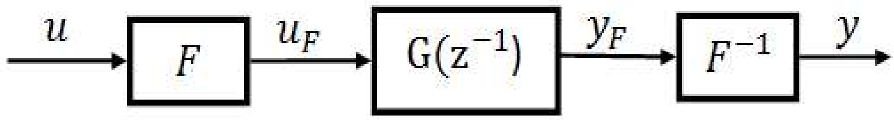

Figure 3.2 Filter of input signal

3.5 Model structures

In practical measurements, there is always measurement noise. This problem is shown in Figure 3.3:

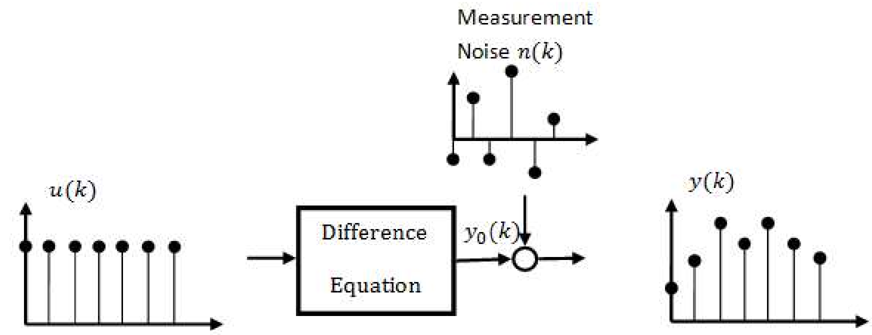

Figure 3.3 Input and noise

The deterministic system behavior is directed through the input $u(k)$ and the output $y_0(k)$. Due to imperfections, measurement noise $n(k)$ always comes to the deterministic (ideal) output and only the real output can be measured.

$$y(k) = y_0(k) + n(k) \tag{3.5}$$

Since neither the measurement noise $n(k)$ nor the ideal deterministic output $y_0(k)$ can be measured, one always has incorrect output data. An attempt is made to approximate the noise model (measurement noise) with the help of white noise.

These so-called noise models always have the same structure. White noise is present at the input of a linear discrete transfer function and colored noise is obtained at the output. The corresponding block diagram is shown in Figure 3.4.

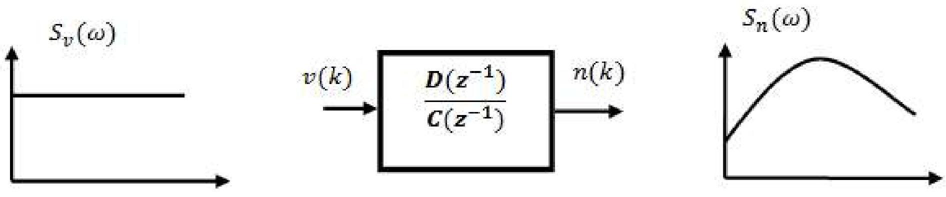

Figure 3.4 Corresponding block diagram

However, it should be clear that these noise models, like the modeling, which only adds noise after the system output, are purely theoretical assumptions. In fact, many noise sources act on the system, and the appropriate choice of a noise model contributes greatly to the success of experimental modeling.

A noise model is necessary to describe a real measurement noise. However, the structure and the parameters of this noise model are not fixed a priori, but must first be determined together with the transfer function of the unknown dynamic system.

The most general model, which includes all other than special cases, is the Box-Jenkins model. The output $Y(z)$ is described in the direct frequency domain by;

$$Y(z) = \frac{B(z^{-1})}{A(z^{-1})}U(z) + \frac{D(z^{-1})}{C(z^{-1})}V(z) \qquad (\mathbf{3.6})$$

where $U(z)$ is the system input and $V(z)$ is white noise. In this model, the parameters of 4 different polynomials A, B, C and D have to be estimated.

The simplest structure is the Output Error (OE) model, in which the transfer function of the noise model is 1, which means that white noise is added directly to the output:

$$Y(z) = \frac{B(z^{-1})}{A(z^{-1})}U(z) + V(z) \qquad (\mathbf{3.7})$$

This means that only the polynomials A and B have to be estimated; the noise model is set to 1 from the start.

Another widely used variant is the ARMAX model (Auto regression with moving average and extra input). A common denominator is assumed for both transfer functions and the number of unknown polynomials is 3.

$$Y(z) = \frac{B(z^{-1})}{A(z^{-1})}U(z) + \frac{D(z^{-1})}{A(z^{-1})}V(z) \qquad (\mathbf{3.8})$$

Another simplification of the ARMAX model is the ARX model. The numerator polynomial of the noise model D = 1 is also chosen here; thus the formula;

$$Y(z) = \frac{B(z^{-1})}{A(z^{-1})}U(z) + \frac{1}{A(z^{-1})}V(z) \qquad (3.9)$$

again only 2 unknown polynomials remain. Note that the ARX and OE models only differ in the noise model.

The structure of the models in the form of block diagrams can be seen in Figure 3.5. In addition to a transfer function for the system, all models have a noise model of varying complexity.

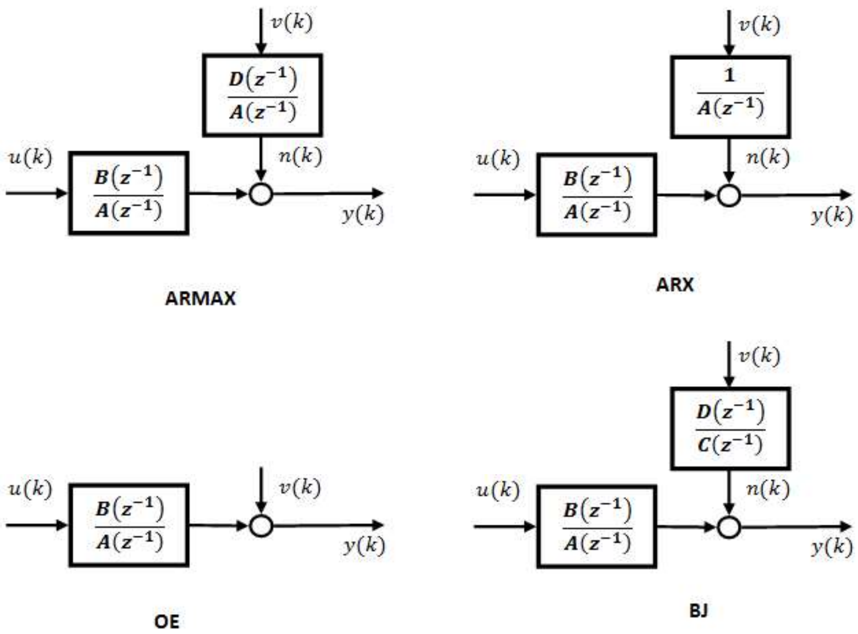

Figure 3.5 Noise model structures

In general, the following can be said about the selection of the suitable model structure:

The ARX model is simple and the parameters of the transfer function can be estimated very efficiently because of the structure. The obvious disadvantage is that the poles of the transfer function completely define the noise filter. This can lead to an unnecessarily high order of the transfer functions. If the measurement noise is only present to a lesser extent, then this leads to good results [15].

The ARMAX model provides a more flexible noise model and can therefore deliver good results in many cases. It can also be calculated efficiently [16].

The OE model only describes the system dynamics and does not specifically deal with the noise. This model delivers good results even if the noise signal is not white, but with increased numerical effort [17].

The BJ model has the most flexible structure and can therefore generally deliver the best results. However, for a good estimation, it also needs the longest data records, since most of the parameters have to be estimated and non-linearly optimized [18].

In addition, one should keep in mind that real noise can also have an effect close to the input; in this case, it is obvious that the noise model has the same poles as the system model. However, if there is real measurement noise, a BJ model is more effective.

At the same time as the decision on the structure, one must also make the decision on the model order. The order is also an a priori assumption and can only be checked afterwards. Therefore, it can only be compared and contrasted models of different orders.

3.6 Identification

The input which is used for identification of the system is a PRBS (Pseudo Random Binary Sequence). A data set, which is collected separately, is used for the system validation. This has a 0.2 A Amplitude and 25 Hz frequency The input is limited because the motion of the system is constricted. The output shaft can only rotate ±30°.25 Hz frequency is chosen because one of the system pole expected around 62 rad/sec (10 Hz).In Figure 3.6 and Figure 3.7 are shown the input PRBS signal and the spectral density of the signal. The output of the system is the fin angle which is shown in Figure 3.8.

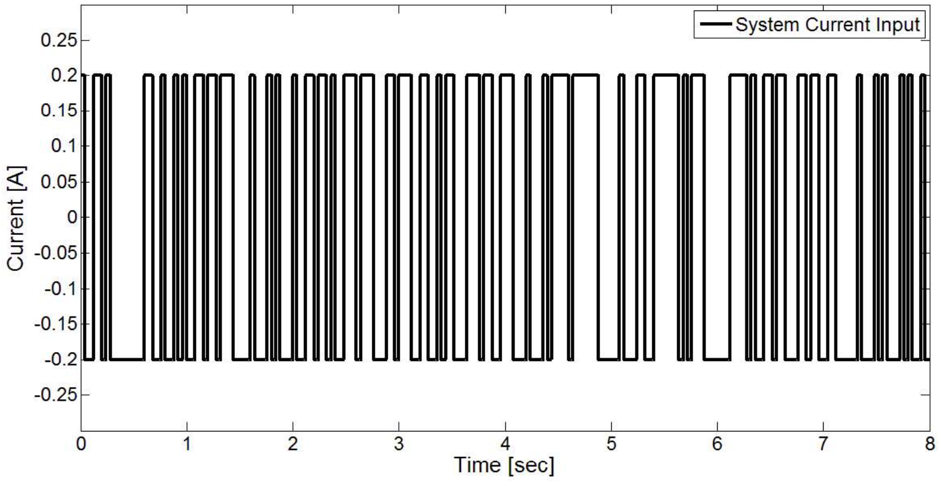

Figure 3.6 System current input

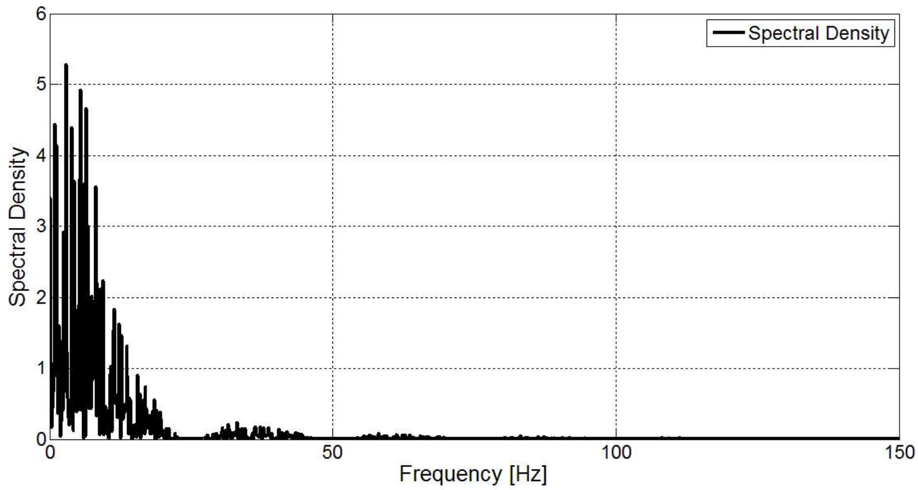

Figure 3.7 Spectral density

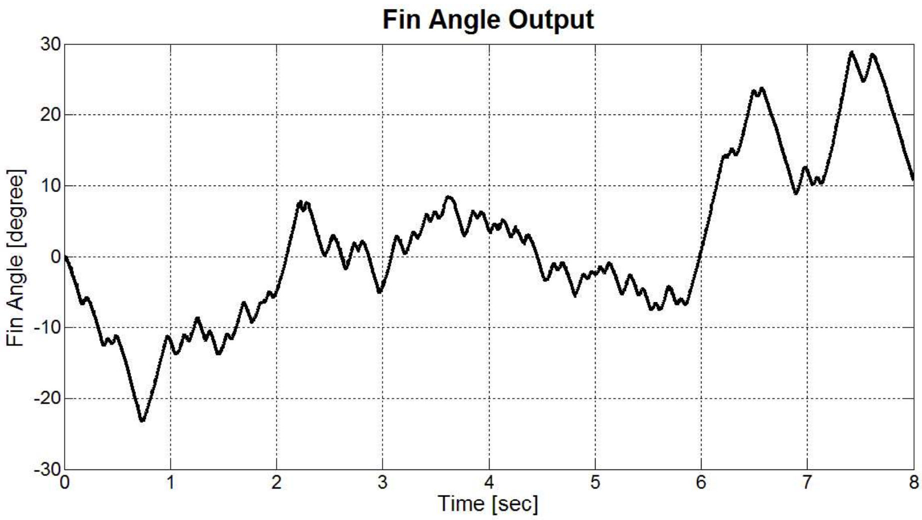

Figure 3.8 System output

For the system identification, 37 different inputs were generated and these inputs were given to the system. As noise model is BJ method is chosen because of the sensor noise. The best 10 VAF result is given in Table 3.1. With obtained outputs system identification process is done. Because of the sensor noise, BJ method gives the best results. As model order is a polynomial with coefficients (1 4 4 2 1) chosen.

As a scale of precision of the suggested model, the Variance Accounted For (VAF), which can be calculated by the formula below [19].

$$VAF = \left(1 - \frac{VAR(y(t) - \hat{y}(t))}{VAR(y(t))}\right) x\ 100 \qquad \mathbf{(3.10)}$$

here;

$y(t)$: Measured data.

$\hat{y}(t)$: Estimated data.

Table 3.1 VAF of 10 best data set

Data Pair	VAF %
1	85,4
2	73,7
3	71
4	72
5	79,8
6	72,6
7	94,8
8	75,7
9	86,2
10	82

VAF is frequently used to confirm the precision of a model, to compare the measured output with the output of the model which is calculated via system identification.

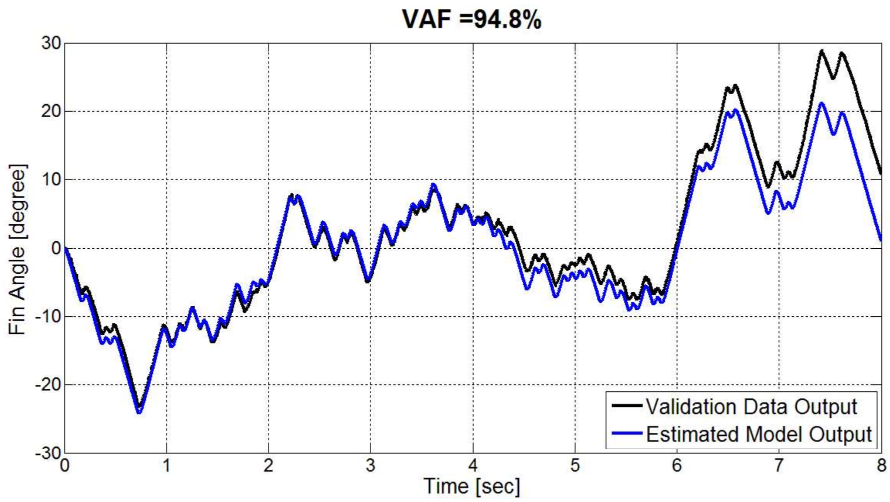

Figure 3.9 Best VAF result of validation data (Data pair 7) and estimated data

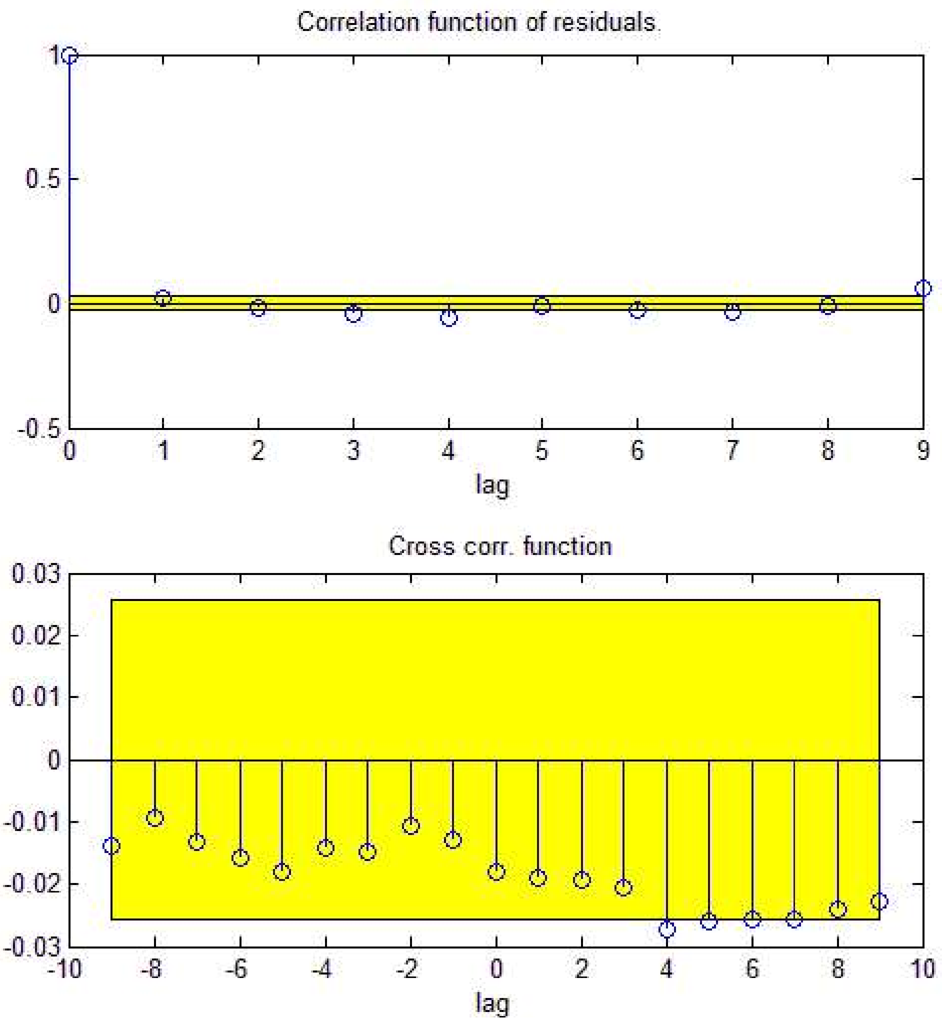

Figure 3.10 Correlation of training data and cross- correlation of estimated data and training data

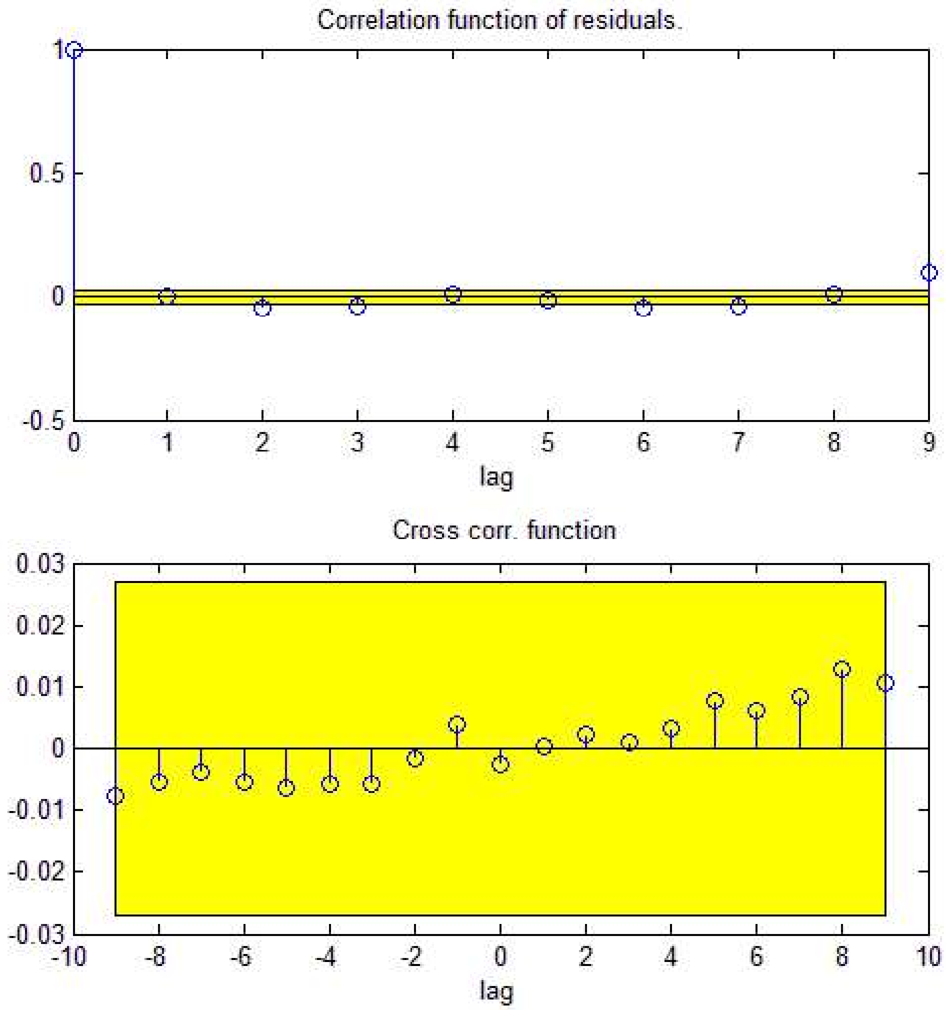

Figure 3.11 Correlation of validation data and cross- correlation of estimated output and validation data

As shown in Figure 3.9, Figure 3.10, and Figure 3.11 the percentage coherence of the model outputs obtained by using the training data and the validation data output is high. The fact that the correlation test results remain within the band indicates that the estimated model was obtained safely. The transfer function between motor current and fin angle is:

$$G_{plant}(s) = \frac{281.6}{0.02092\mathrm{s}^2 + \mathrm{s}}\left[\frac{\mathrm{degree}}{\mathrm{A}}\right] \quad \mathbf{(3.11)}$$

If this plant transfer function with Laplace transfer of the dynamic equation of FAS is equalized by considering the system is linear;

$$J_F \cdot \ddot{\theta}_F(t) + B_F \cdot \dot{\theta}_F(t) = N \cdot K_t \cdot i(t) \tag{3.12}$$

$$J_F \cdot \theta_F \cdot s^2 + B_F \cdot \theta_F \cdot s = N \cdot K_t \cdot i \tag{3.13}$$

this Laplace transformed equation could be written as a transfer function. The input is the motor current and the output is the fin angle.

$$G_{plant}(s) = \frac{\theta_F}{i} = \frac{N \cdot K_t}{J_F \cdot s^2 + B_F \cdot \mathrm{s}} = \frac{\frac{N \cdot K_t}{B_F}}{\frac{J_F}{B_F} \cdot s^2 + s} = \frac{281.6}{0.02092\mathrm{s}^2 + \mathrm{s}} \tag{3.14}$$

The transmission ratio of the system$N$is considered as 78 and the torque constant of the DC motor K_t is 0.1 Nm/A. Then according to the fin axis moment of inertia of the system J_F and viscous friction constant B_F could be calculated as:

$$J_F = 5{,}79 \cdot 10^{-4} kg \cdot\ m^2 \tag{3.15}$$

$$B_F = 0{,}0277 Nm \cdot s/degree \tag{3.16}$$

3.7 Calculation of System Inertia

In order to calculate the projected inertia respect to fin axis of the system, it has to be added to every link and every rotating component, because the whole system is driven by motor. Fin axis and motor axis are not on the same line. Parts of the system could be seen in Figure 3.12.

The moment of inertia equation of the ballscrew-nut could be derived from the kinetic energy equation for both systems because of translational motion. $\dot{\theta}_M$ is the velocity of the motor.

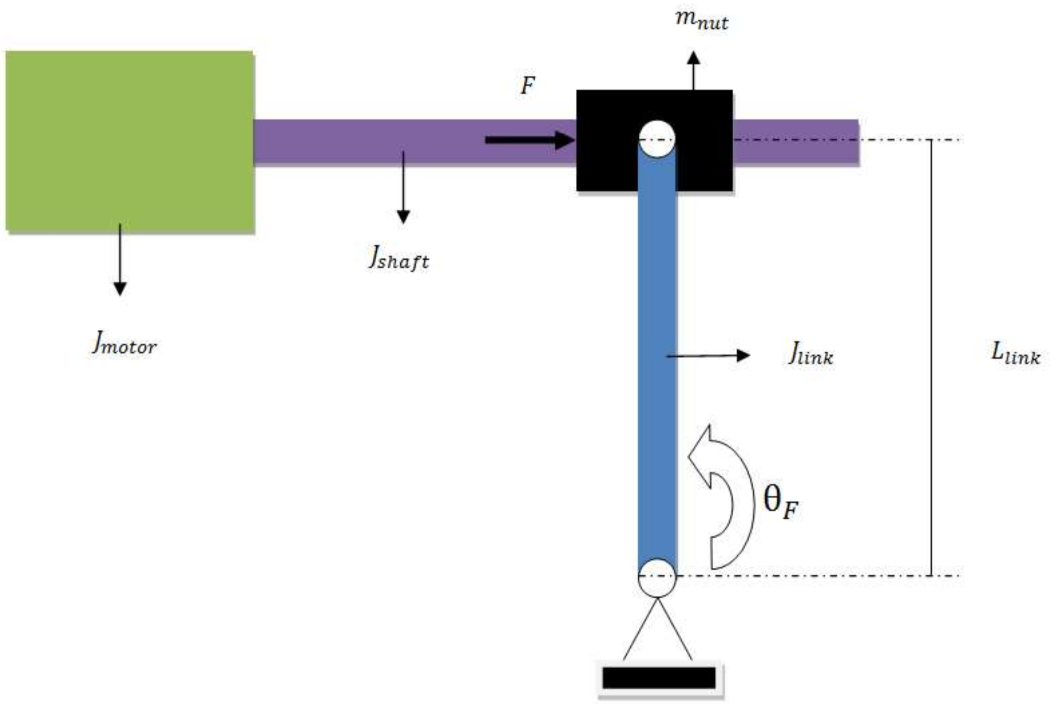

Figure 3.12 Moment of inertia of the system

$$\frac{1}{2}m_{equivalent}\cdot {v_{nut}}^2=\frac{1}{2}(J_{motor}+J_{shaft})\cdot {\dot{\theta}_M}^{2}+\frac{1}{2}(m_{nut})\cdot {v_{nut}}^2 \quad \mathbf{(3.17)}$$

The v_{nut} is the velocity of the nut. The $m_{equivalent}$ is the equivalent mass of the components on the motor axis. The transmission ratio between shaft and nut is ρ=3/2π = 0.4775 mm/rad. Therefore;

$$\frac{1}{2}m_{equivalent}\cdot (\rho\cdot\dot{\theta}_M)^2=$$

$$=\frac{1}{2}(J_{motor}+J_{shaft})\cdot {\dot{\theta}_M}^{2}+\frac{1}{2}(m_{nut})\cdot (\rho\cdot\dot{\theta}_M)^2 \quad \mathbf{(3.18)}$$

$$m_{equivalent}=\frac{(J_{motor}+J_{shaft})}{\rho^2}+m_{nut} \quad \mathbf{(3.19)}$$

$$m_{nut}=6.632\cdot 10^{-2}\text{kg} \quad \mathbf{(3.20)}$$

J_{motor} and $J_{shaft}$are taken from NX software:

$$J_{motor} = 1{,}5520 \cdot 10^{-5}\text{kg} \cdot\ m^2 \qquad (\mathbf{3.21})$$

$$J_{shaft} = 3{,}30 \cdot 10^{-6}\text{kg} \cdot\ m^2 \qquad (\mathbf{3.22})$$

$$m_{equivalent} = 6.64 \cdot 10^{-2} kg \qquad (\mathbf{3.23})$$

Another kinetic energy equation for the fin axis can be written;

$$\frac{1}{2} J_{equivalent} \cdot \dot{\theta}_F{}^2 = \frac{1}{2} J_{link} \cdot \dot{\theta}_F{}^2 + \frac{1}{2} m_{equivalent} \cdot v_{nut}{}^2 \qquad (\mathbf{3.24})$$

here is $J_{equivalent}$ the inertia of whole system reduced on the fin axis and v_{nut} as a function of $\dot{\theta}_F$:

$$v_{nut} = L_{link} \cdot \dot{\theta}_F \qquad (\mathbf{3.25})$$

$$\frac{1}{2} J_{equivalent} \cdot \dot{\theta}_F{}^2 = \frac{1}{2} J_{link} \cdot \dot{\theta}_F{}^2 + \frac{1}{2} m_{equivalent} \cdot (L_{Link} \cdot \dot{\theta}_F)^2 \qquad (\mathbf{3.26})$$

$$J_{equivalent} = J_{link} + m_{equivalent} \cdot L_{link}{}^2 \qquad (\mathbf{3.27})$$

J_{Link} could be taken by using NX software:

$$J_{Link} = 3{,}2910 \cdot 10^{-4}\ kg \cdot\ m^2 \qquad (\mathbf{3.28})$$

and

$$L_{Link} = 0.060\ m \qquad (\mathbf{3.29})$$

$$J_{equivalent} = J_{F\_calculated} = 5{,}6815 \cdot 10^{-4}\ kg \cdot\ m^2 \qquad (\mathbf{3.30})$$

Calculated inertia is similar to inertia which is founded with system identification method. The reason for this difference could be rolling components in bearing.

CHAPTER 4

CONTROLLER DESIGN

The nonlinear behavior of electromechanical actuators represents a difficult question in designing ideal controllers for these actuators. Problems in identifying a precise model of naturally nonlinear dynamics make controller design more sophisticated. Many scientists have used modern control methods to upgrade the system performance especially in tracking and motion control capability [20].

When designing a state feedback control, all existing cross-couplings of a system are taken into account. For this, it is necessary to be able to measure all state variables of the system in the ideal case or to estimate them by an observer. The system must be fully controllable for the design. If an observer is to be called in to estimate the states, the system must also be fully observable.

Figure 4.1 illustrates the structure of a state feedback control. The state vector x is fed back to the system inputs u via the feedback matrix K. The system reference is r [19].

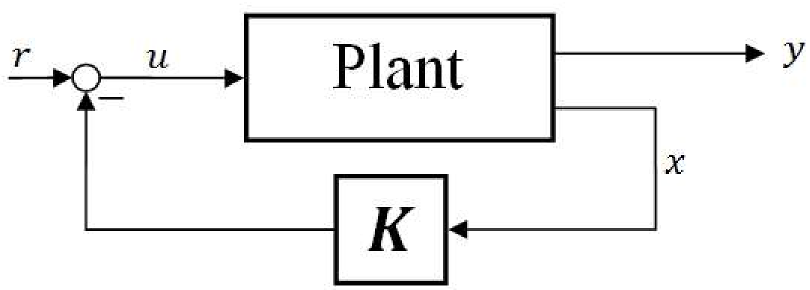

Figure 4.1 General state feedback block diagram

The state space model is described with state feedback according to the following equations:

$$\dot{x} = \mathrm{A}x + \mathrm{B}u \tag{4.1}$$

$$y = \mathrm{C}x + \mathrm{D}u \tag{4.2}$$

Here:

x: State vector (nx1)
y: Output vector (1x1)
u: Input vector (1x1)
A: State matrix(nxn)
B: Input matrix (nx1)
C: Output matrix(1xn)
D: Feedthrough matrix(1x1)
$\dot{x}$: Time derivative of vector$x$(nx1)

The complete controllability of a system can be checked with the criterion proposed by Kalman. This criterion relates to the controllability matrix S_C which is an (nxn) matrix. If the system has only one input, the matrix S_C is square.

$$S_C = (B \;\; AB \;\; A^2B \ldots A^{n-1}B) \tag{4.3}$$

The system (A, B) is fully controllable if and only if the controllability matrix S_C has the rank n:

$$Rank\ S_C = n \tag{4.4}$$

The observability criteria and the controllability criteria are very similar. It becomes obvious that observability is a dual property to controllability so that the following investigations can be made much more briefly. The Kalman-criterion refers to the observability matrix

$$S_O = \begin{pmatrix} C \\ CA \\ CA^2 \\ . \\ . \\ . \\ CA^{n-1} \end{pmatrix} \qquad \mathbf{(4.5)}$$

which is an (nxn) matrix. It is square if the system is only one output. The system (A, C) is completely observable if and only if the observability matrix S_O has rank n.

$$Rank\ S_O = n \qquad \mathbf{(4.6)}$$

A system is asymptotically stable if its states are at a finite initial deflection for t → ∞ strive towards 0.

A linear system is asymptotically stable if and only if all real part of eigenvalues of the system matrix A lie in the left half-plane, i.e.

$Re\{\lambda_i\} < 0$ for all $i = 1,2, \dots, n$

4.1 State Feedback Controller

Dynamic equation of FAS is used to control the system:

$$J_F\ddot{\theta}_F(t) + B_F\dot{\theta}_F(t) = NK_t i(t) \qquad \mathbf{(4.7)}$$

State space system equations could be written as;

$$\dot{x} = Ax + Bu \qquad \mathbf{(4.8)}$$

$$y = Cx + Du \qquad \mathbf{(4.9)}$$

$$u = r - Kx \qquad \mathbf{(4.10)}$$

The states are chosen, the first state is the fin angle and the second state is the angular speed of the fin. And state space block diagram could be seen in Figure 4.2.

$$x_1 = \theta_F \qquad \mathbf{(4.11)}$$

$$x_2 = \dot{\theta}_F \tag{4.12}$$

$$\dot{x}_1 = x_2 \tag{4.13}$$

$$\dot{x}_2 = -\frac{B_F}{J_F}x_2 + \frac{NK_t}{J_F}\cdot i \tag{4.14}$$

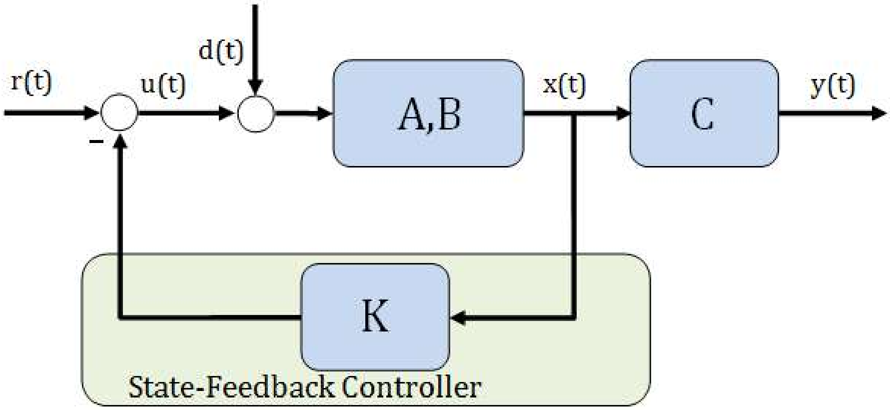

Figure 4.2 State feedback controller block diagram

State feedback matrices could be written as below:

$$\boldsymbol{A} = \begin{bmatrix} 0 & 1 \\ 0 & -\frac{B_F}{J_F} \end{bmatrix} \tag{4.15}$$

$$\boldsymbol{B} = \begin{bmatrix} 0 \\ \frac{NK_t}{J_F} \end{bmatrix} \tag{4.16}$$

$$\boldsymbol{C} = [1 \quad 0] \tag{4.17}$$

$$\boldsymbol{D} = [0] \tag{4.18}$$

$$\boldsymbol{K} = [k_1 \quad k_2] \tag{4.19}$$

Closed loop system equation is [21]:

$$\frac{\boldsymbol{Y}(\boldsymbol{s})}{\boldsymbol{R}(\boldsymbol{s})} = \boldsymbol{C}(\boldsymbol{sI} - (\boldsymbol{A} - \boldsymbol{BK}))^{-1}\boldsymbol{B} \tag{4.20}$$

In order to calculate the closed loop equation, the components of the matrices have to be calculated. The calculation is written step by step.

$$\boldsymbol{A}-\boldsymbol{BK}=\begin{bmatrix}0 & 1\\ 0 & -\frac{B_F}{J_F}\end{bmatrix}-\begin{bmatrix}0\\ \frac{NK_t}{J_F}\end{bmatrix}[k_1 \quad k_2] \qquad \mathbf{(4.21)}$$

$$\boldsymbol{A}-\boldsymbol{BK}=\begin{bmatrix}0 & 1\\ 0 & -\frac{B_F}{J_F}\end{bmatrix}-\begin{bmatrix}0 & 0\\ \frac{k_1NK_t}{J_F} & \frac{k_2NK_t}{J_F}\end{bmatrix} \qquad \mathbf{(4.22)}$$

$$\boldsymbol{A}-\boldsymbol{BK}=\begin{bmatrix}0 & 1\\ -\frac{k_1NK_t}{J_F} & -\frac{B_F}{J_F}-\frac{k_2NK_t}{J_F}\end{bmatrix} \qquad \mathbf{(4.23)}$$

for the abbreviation:

$$-\frac{k_1NK_t}{J_F}=a \qquad \mathbf{(4.24)}$$

$$-\frac{B_F}{J_F}-\frac{k_2NK_t}{J_F}=b \qquad \mathbf{(4.25)}$$

Equation 4.22 in new form;

$$\boldsymbol{A}-\boldsymbol{BK}=\begin{bmatrix}0 & 1\\ a & b\end{bmatrix} \qquad \mathbf{(4.26)}$$

The difference of s times identity matrix and equation 4.25;

$$\boldsymbol{sI}-(\boldsymbol{A}-\boldsymbol{BK})=\begin{bmatrix}s & 0\\ 0 & s\end{bmatrix}-\begin{bmatrix}0 & 1\\ a & b\end{bmatrix} \qquad \mathbf{(4.27)}$$

$$\boldsymbol{sI}-(\boldsymbol{A}-\boldsymbol{BK})=\begin{bmatrix}s & -1\\ -a & s-b\end{bmatrix} \qquad \mathbf{(4.28)}$$

the inverse of equation 4.27

$$(\boldsymbol{sI}-(\boldsymbol{A}-\boldsymbol{BK}))^{-\mathbf{1}}=\begin{bmatrix}s & -1\\ -a & s-b\end{bmatrix}^{-1} \qquad \mathbf{(4.29)}$$

the inverse can be calculated with the help of determinant:

$$(\boldsymbol{sI}-(\boldsymbol{A}-\boldsymbol{BK}))^{-\boldsymbol{1}}=\frac{1}{s(s-b)-a}\begin{bmatrix} s-b & 1\\ a & s\end{bmatrix} \quad (\boldsymbol{4.30})$$

$$(\boldsymbol{sI}-(\boldsymbol{A}-\boldsymbol{BK}))^{-\boldsymbol{1}}=\begin{bmatrix} \frac{s-b}{s(s-b)-a} & \frac{1}{s(s-b)-a}\\ \frac{a}{s(s-b)-a} & \frac{s}{s(s-b)-a}\end{bmatrix} \quad (\boldsymbol{4.31})$$

Output matrix C times equation 4.30;

$$\boldsymbol{C}(\boldsymbol{sI}-(\boldsymbol{A}-\boldsymbol{BK}))^{-\boldsymbol{1}}=[1 \quad 0]\begin{bmatrix} \frac{s-b}{s(s-b)-a} & \frac{1}{s(s-b)-a}\\ \frac{a}{s(s-b)-a} & \frac{s}{s(s-b)-a}\end{bmatrix} \quad (\boldsymbol{4.32})$$

$$\boldsymbol{C}\big(\boldsymbol{sI}-(\boldsymbol{A}-\boldsymbol{BK})\big)^{-\boldsymbol{1}}=\begin{bmatrix} \frac{s-b}{s(s-b)-a} & \frac{1}{s(s-b)-a}\end{bmatrix} \quad (\boldsymbol{4.33})$$

Equation 4.32 times B matrix;

$$\boldsymbol{C}(\boldsymbol{sI}-(\boldsymbol{A}-\boldsymbol{BK}))^{-\boldsymbol{1}}\boldsymbol{B}=\begin{bmatrix} \frac{s-b}{s(s-b)-a} & \frac{1}{s(s-b)-a}\end{bmatrix}\begin{bmatrix} 0\\ \frac{NK_t}{J_F}\end{bmatrix} \quad (\boldsymbol{4.34})$$

$$\boldsymbol{C}(\boldsymbol{sI}-(\boldsymbol{A}-\boldsymbol{BK}))^{-\boldsymbol{1}}\boldsymbol{B}=\frac{\frac{NK_t}{J_F}}{s(s-b)-a} \quad (\boldsymbol{4.35})$$

$$\boldsymbol{C}(\boldsymbol{sI}-(\boldsymbol{A}-\boldsymbol{BK}))^{-\boldsymbol{1}}\boldsymbol{B}=\frac{\frac{N\cdot K_t}{J_F}}{s^2-bs-a} \quad (\boldsymbol{4.36})$$

Equation 4.23 and 4.24 in equation 4.35

$$\boldsymbol{C}(\boldsymbol{sI}-(\boldsymbol{A}-\boldsymbol{BK}))^{-\boldsymbol{1}}\boldsymbol{B}=\frac{\frac{NK_t}{J_F}}{s^2-\left(-\frac{B_F}{J_F}-\frac{k_2NK_t}{J_F}\right)s-\left(-\frac{k_1NK_t}{J_F}\right)} \quad (\boldsymbol{4.37})$$

$$\boldsymbol{C}(\boldsymbol{sI}-(\boldsymbol{A}-\boldsymbol{BK}))^{-\boldsymbol{1}}\boldsymbol{B}=\frac{\frac{NK_t}{J_F}}{s^2+\left(\frac{B_F}{J_F}+\frac{k_2NK_t}{J_F}\right)s+\left(\frac{k_1NK_t}{J_F}\right)} \quad (\boldsymbol{4.38})$$

Finally, the closed loop transfer function can be written as:

$$\frac{\boldsymbol{Y(s)}}{\boldsymbol{R(s)}} = \boldsymbol{C}\big(\boldsymbol{sI} - (\boldsymbol{A} - \boldsymbol{BK})\big)^{-1}\boldsymbol{B} = \frac{\frac{NK_t}{J_F}}{s^2 + \left(\frac{B_F}{J_F} + \frac{k_2 NK_t}{J_F}\right)s + \left(\frac{k_1 NK_t}{J_F}\right)} \qquad \textbf{(4.39)}$$

If the poles are at -150 ± 150i located, with this placement it is aimed a system with 33.76 Hz (212.13 rad/sec) natural frequency and damping coefficient 0.707. Than the transfer function is;

$$\frac{\boldsymbol{Y(s)}}{\boldsymbol{R(s)}} = \frac{\frac{NK_t}{J_F}}{s^2 + \left(\frac{B_F}{J_F} + \frac{k_2 NK_t}{J_F}\right)s + \left(\frac{k_1 NK_t}{J_F}\right)} = \frac{13470}{s^2 + 300s + 45000} \qquad \textbf{(4.40)}$$

The command *place* in Matlab is used to find the controller coefficients.

$$K = [k_1 \;\; k_2] = [3.3404 \quad 0.0187] \qquad \textbf{(4.41)}$$

For a good tracking performance, it must be guaranteed:

$$u = r - Kx \qquad \textbf{(4.42)}$$

$$y(t) \approx r(t) \;\; as \;\; t \to \infty \qquad \textbf{(4.43)}$$

if the final value theorem is in frequency domain written:

$$\lim_{t \to \infty} y(t) = \lim_{s \to 0} \mathrm{sY(s)} \qquad \textbf{(4.44)}$$

Thus, for good performance for step response:

$$sY(s) \approx sR(s) \text{as s} \to 0 \;\; \left.\frac{\mathrm{Y(s)}}{\mathrm{R(s)}}\right|_{s=0} = 1 \qquad \textbf{(4.45)}$$

So, for good performance, the transfer function from $R(s)$ to $Y(s)$should be approximately 1.

$$\left.\frac{\mathrm{Y(s)}}{\mathrm{R(s)}}\right|_{s=0} = \frac{13470}{s^2 + 300s + 45000} = \frac{13470}{45000} \neq 1 \qquad \textbf{(4.46)}$$

In this case, reference could not be tracked. This can be seen in Figure 4.3. From the equation could be understood that the numerator and the constant term of the denominator must be the same. Therefore the reference has to multiplied by a gain $\tilde{N}$.

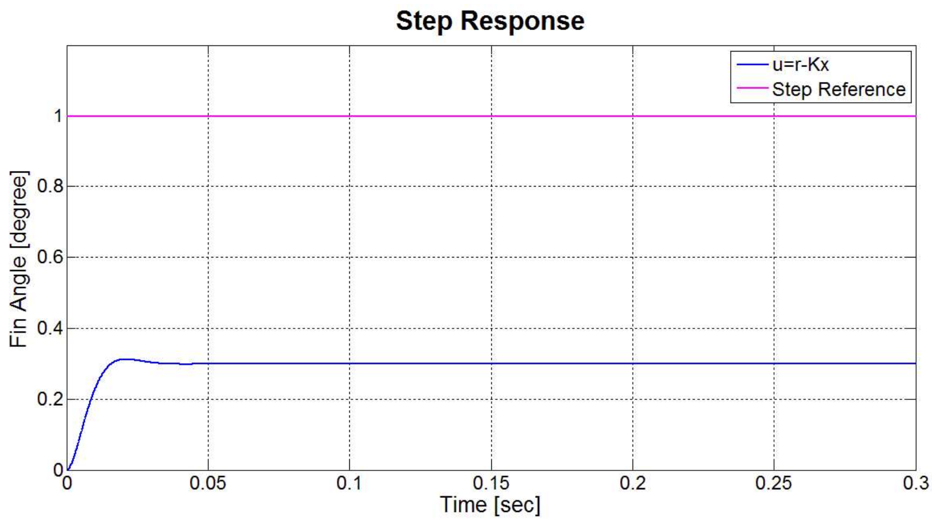

Figure 4.3 Step response

$$u = \tilde{N}r - Kx \tag{4.47}$$

$\tilde{N}$ is an additional gain used to scale the closed-loop transfer function (Figure 4.4).

$$\dot{x} = (A - BK)x + B\tilde{N}r \tag{4.48}$$

$$y = Cx \tag{4.49}$$

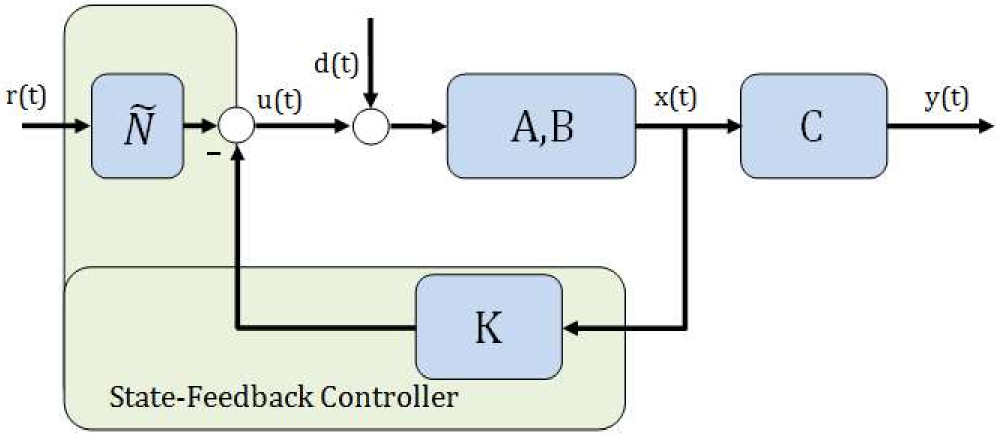

Figure 4.4 State feedback controller with additional gain

Now the closed-loop transfer function is in a new form:

$$\frac{\mathrm{Y(s)}}{\mathrm{R(s)}} = C(sI - (A - BK))^{-1}B\widetilde{N} \tag{4.50}$$

To realize good tracking Ñ could be calculated:

$$\left.\frac{\mathrm{Y(s)}}{\mathrm{R(s)}}\right|_{\mathrm{s=0}} = 1 \tag{4.51}$$

$$\widetilde{N} = \frac{45000}{13470} \tag{4.52}$$

$$\frac{\mathrm{Y(s)}}{\mathrm{R(s)}} = \frac{\frac{NK_t}{J_F}\widetilde{N}}{s^2 + \left(\frac{B_F}{J_F} + \frac{k_2NK_t}{J_F}\right)s + \left(\frac{k_1NK_t}{J_F}\right)} = \frac{45000}{s^2 + 300s + 45000} \tag{4.53}$$

$$\left.\frac{\mathrm{Y(s)}}{\mathrm{R(s)}}\right|_{\mathrm{s=0}} = \frac{45000}{s^2 + 300s + 45000} = \frac{45000}{45000} = 1 \tag{4.54}$$

Numerator and the constant term of the denominator must be equal.

$$\frac{\widetilde{N}NK_t}{J_F} = \frac{k_1NK_t}{J_F} \tag{4.55}$$

Therefore $\widetilde{N}$ is equal k_1.This additional gain is also written in reference [22].

$$\widetilde{N} = 3.3404 \quad (4.56)$$

$$\frac{45000}{s^2 + 300s + 45000} = \frac{{\omega_n}^2}{s^2 + 2\xi\omega_n s + {\omega_n}^2} \quad (4.57)$$

Based on this transfer function, the natural frequency of the system is found as 212.13 rad/sec.

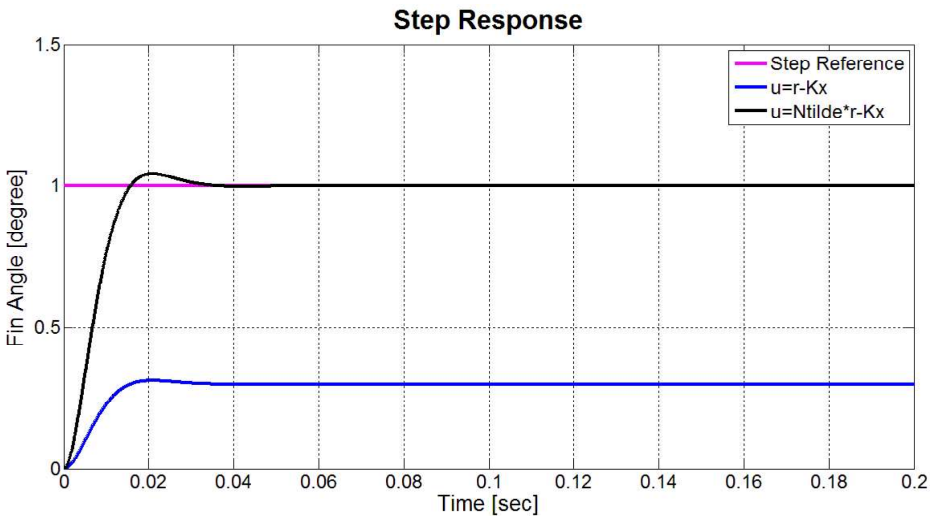

Figure 4.5 Step response

When a step reference is given to closed-loop transfer function in the simulation environment, it is seen that the system response tracks the reference (Figure 4.5). The improved controller has no steady-state error after step response but at 0.1 seconds 1 ampere disturbance in form of motor current applied (Figure 4.6 and Figure 4.7). Because of this disturbance, the controller loses out the reference tracking (Figure 4.7).

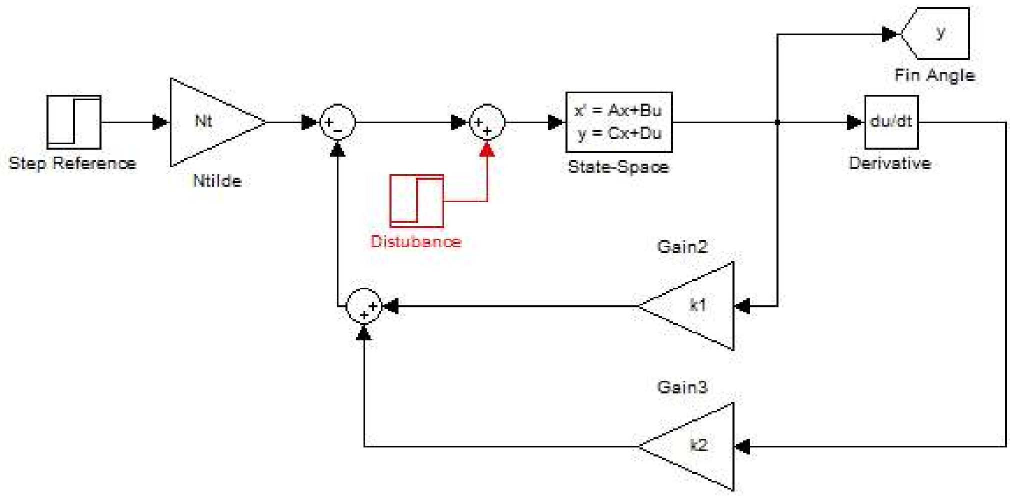

Figure 4.6 Simulink diagram of state feedback controller

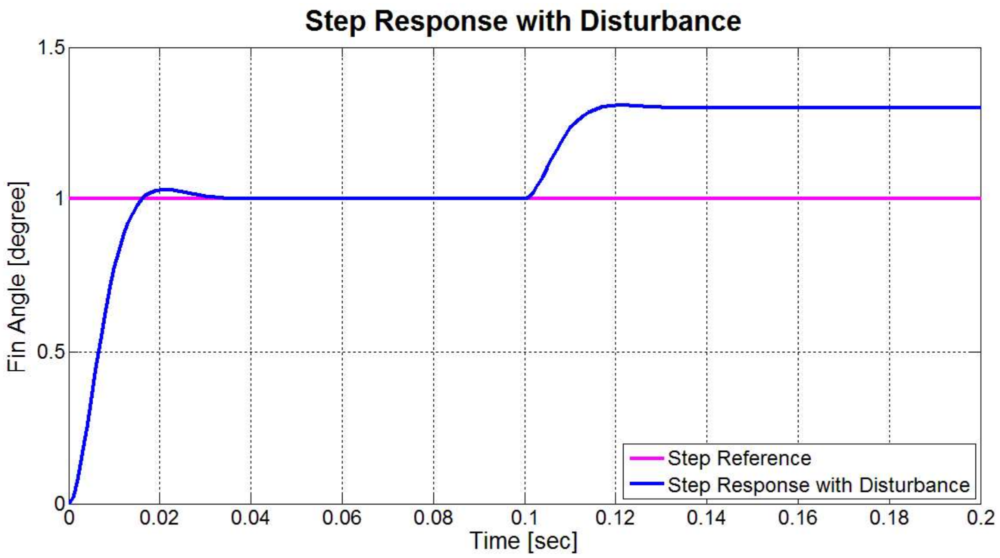

Figure 4.7 Step response with disturbance

To solve this reference tracking problem an outer loop with an integral behavior is added. Because, there was no integral behavior in designed state space controller. The principle of this method in the continuous-time system is:

$$u(t) = -Kx(t) + H\widetilde{N}\int_0^t \big(r(\tau) - y(\tau)\big)d\tau \qquad (\mathbf{4.58})$$

H is the new gain, which is in integral action used. From the equation 4.58, the improved controller block diagram of the system turns into the shape shown in Figure 4.8.

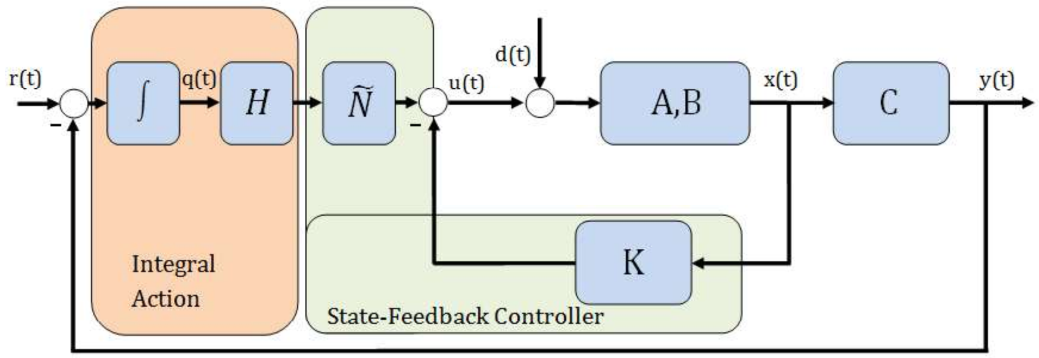

Figure 4.8 State feedback controller with integral action

In this case, the state-space equation of the improved system is;

$$\frac{d}{dt}\begin{bmatrix} x(t) \\ q(t) \end{bmatrix} = \begin{bmatrix} A & 0 \\ C & 0 \end{bmatrix}\begin{bmatrix} x(t) \\ q(t) \end{bmatrix} + \begin{bmatrix} B \\ 0 \end{bmatrix} u(t) \tag{4.59}$$

$$y(t) = \begin{bmatrix} C & 0 \end{bmatrix}\begin{bmatrix} x(t) \\ q(t) \end{bmatrix} \tag{4.60}$$

In order to calculate the new closed-loop transfer function;

$$\frac{\mathrm{Y_{new}(s)}}{\mathrm{R(s)}} = \frac{\mathrm{C(sI-(A-BK))^{-1}B}\tilde{N}_{new}\mathrm{H}\frac{1}{\mathrm{s}}}{1+\mathrm{C(sI-(A-BK))^{-1}B}\tilde{N}_{new}\mathrm{H}\frac{1}{\mathrm{s}}} \tag{4.61}$$

$$\frac{\mathrm{Y_{new}(s)}}{\mathrm{R(s)}} = \frac{\frac{NK_t}{J_F}\tilde{N}_{new}H}{s^3 + \left(\frac{B_F}{J_F} + \frac{k_{2new}NK_t}{J_F}\right)s^2 + \left(\frac{k_{1new}NK_t}{J_F}\right)s + \frac{NK_t}{J_F}\tilde{N}_{new}H} \tag{4.62}$$

Now the system has third order and a pole must be chosen and placed. The third pole is placed at the point -180 on the real axis, which is faster than other pole pair. The new closed-loop transfer function is:

$$\frac{\mathrm{Y_{new}(s)}}{\mathrm{R(s)}} = \frac{8100000}{s^3 + 480s^2 + 99000s + 8100000} \qquad (\mathbf{4.63})$$

And the new controller matrix, coefficient H and $\tilde{N}_{new}$:

$$K_{new} = [k_{1new} \quad k_{2new}] = [7.3488 \quad 0.0321] \qquad (\mathbf{4.64})$$

$$\tilde{N}_{new} = 7.3488 \qquad (\mathbf{4.65})$$

$$H = 81.8187 \qquad (\mathbf{4.66})$$

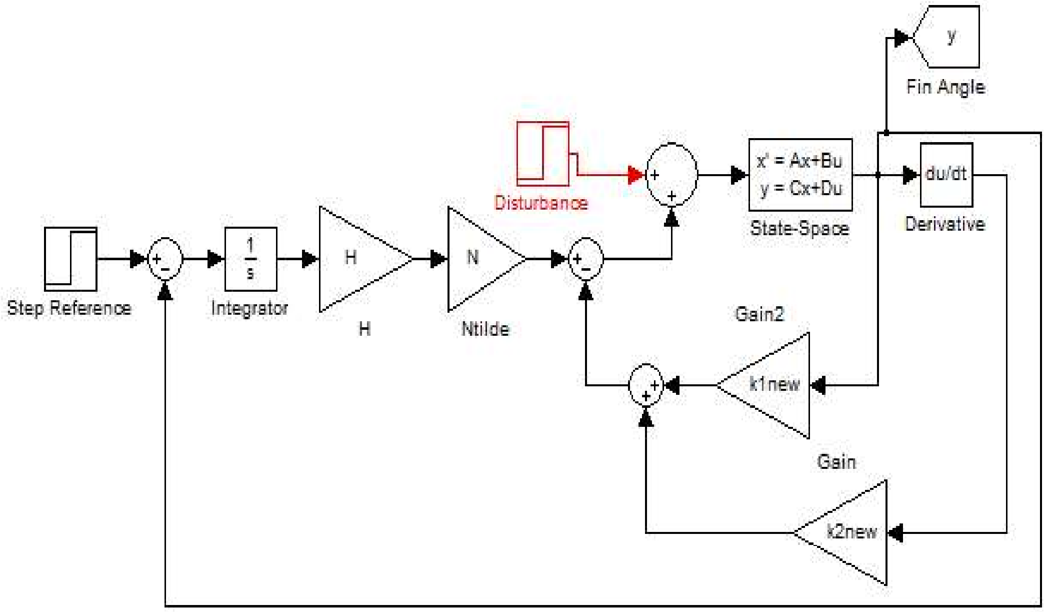

Figure 4.9 Simulink diagram of state feedback controller with integral action

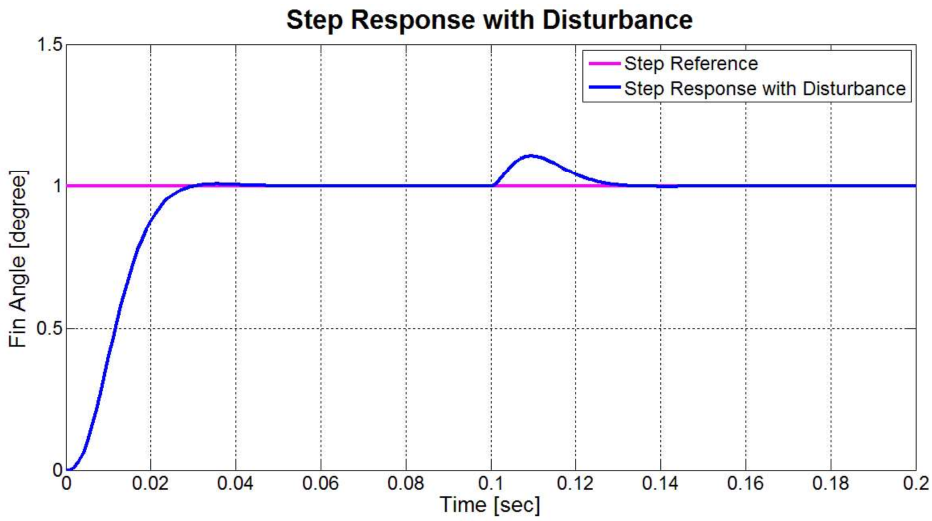

Figure 4.10 Step response of state feedback controller with integral action

The simulink block diagram could be seen in Figure 4.9. When the results of the improved controller are examined, it is seen that it has 0.8 % overshoot and settles at 1 degree before disturbance, tracks the reference after 1-ampere disturbance effect at 0.1 seconds. Motor current before disturbance is nearly 3 ampere. The closed-loop system bandwidth is 22.9 Hz. Step response with the disturbance effect could be seen in Figure 4.10. And the bode plot could be seen in Figure 4.11.

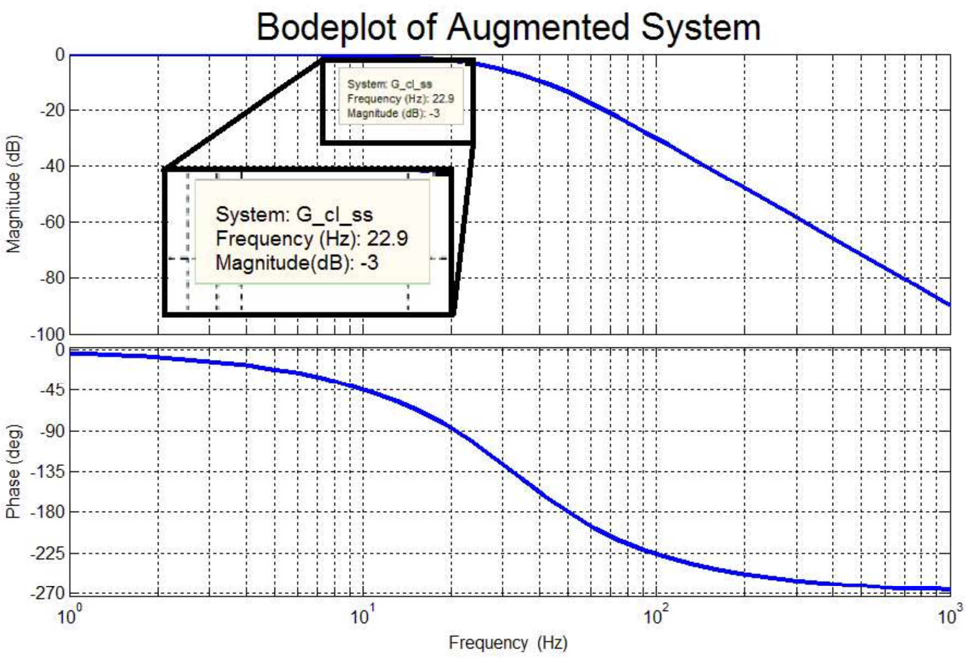

Figure 4.11 Bodeplot of augmented system in equation 4.63

4.2 Controllability

The state-space system without integral action has two states. Therefore the rank of the S_{C1} matrix must equal 2 for controllability:

$$S_{C1} = \begin{bmatrix} 0 & 13470 \\ 13470 & -644490 \end{bmatrix} \quad \mathbf{(4.67)}$$

$$Rank\ S_{C1} = 2 \quad \mathbf{(4.68)}$$

And the state-space system with integral action has three states. Therefore the rank of the S_{C2} matrix must equal 3 for controllability:

$$S_{C2} = \begin{bmatrix} 1 & -480 & 131400 \\ 0 & 1 & -480 \\ 0 & 0 & 1 \end{bmatrix} \quad \mathbf{(4.69)}$$

$$Rank\ S_{C2} = 3 \quad \mathbf{(4.70)}$$

Both systems are controllable.

4.3 Observability

The state-space system without integral action has two states. Therefore the rank of the S_{O1} matrix must equal 2 for observability:

$$S_{O1} = \begin{bmatrix} 0 & 1 \\ 1 & 0 \end{bmatrix} \quad \mathbf{(4.71)}$$

$$Rank\ S_{O1} = 2 \quad \mathbf{(4.72)}$$

The state-space system with integral action has three states. Therefore the rank of the S_{O2} matrix must equal 3 for observability:

$$S_{O2} = \begin{bmatrix} 0 & 0 & 8100000 \\ 0 & 8100000 & 0 \\ 8100000 & 0 & 0 \end{bmatrix} \quad \mathbf{(4.73)}$$

$$Rank\ S_{O2} = 3 \quad \mathbf{(4.74)}$$

Both systems are observable. The observability was not used in the thesis, but this subject was mentioned as it could be used in future studies.

4.4 Stability

The closed-loop system has three poles. All poles of the system present in the left half of the ‘s’ plane. In Figure 4.12is shown the poles of the system.

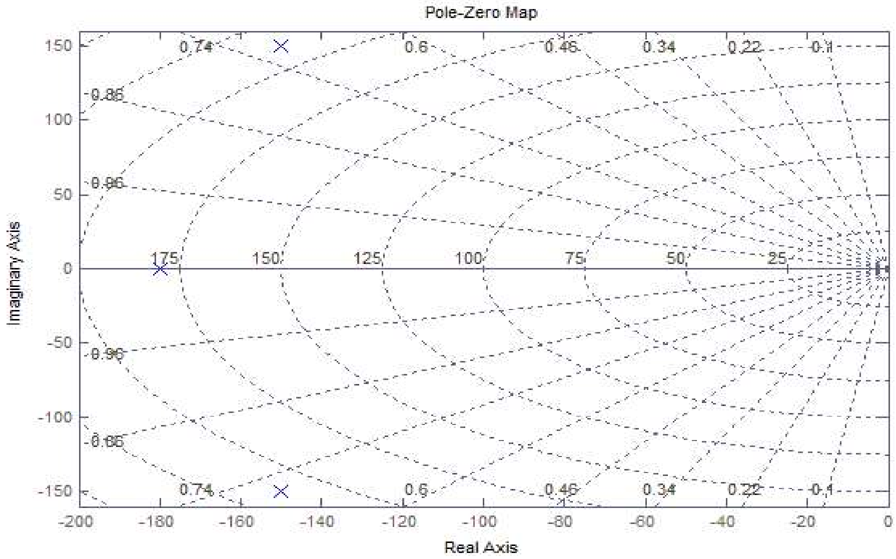

Figure 4.12 Pole zero map of closed loop system of state feedback controller

4.5 PID Controller Design

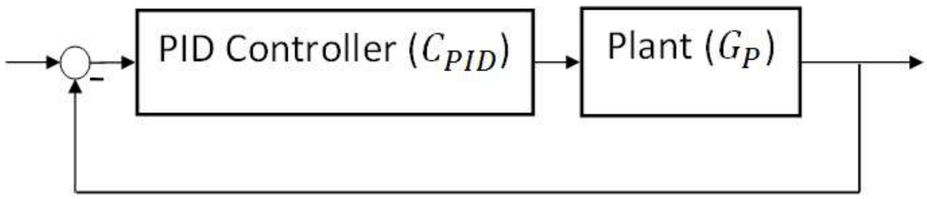

Figure 4.13 Block diagram of PID controller

A general PID controller block diagram could be seen in Figure 4.13. In order to design a PID controller, the same closed-loop poles of the state feedback controller are chosen. The closed-loop system of the PID controlled system has to have the same poles as the previous system. Also, the poles are located at -150 ± 150i and-180 in the complex coordinate system. The PID controller could be written as:

$$C_{PID} = \frac{K_D s^2 + K_P s + K_I}{s} \qquad (\mathbf{4.75})$$

And the plant is:

$$G_{Plant} = \frac{281.6}{0.02092s^2 + s} \tag{4.76}$$

The closed-loop system could be written as:

$$G_{CL} = \frac{C_{PID}G_{Plant}}{1 + C_{PID}G_{Plant}} \tag{4.77}$$

Equation 4.70 and 4.71 in equation 4.72;

$$G_{CL} = \frac{\frac{281.6\,(K_D s^2 + K_P s + K_I)}{0.02092s^3 + s^2}}{\frac{0.02092s^3 + s^2 + 281.6\,(K_D s^2 + K_P s + K_I)}{0.02092s^3 + s^2}} \tag{4.78}$$

$$G_{CL} = \frac{281.6\,(K_D s^2 + K_P s + K_I)}{0.02092s^3 + (1 + 281.6\,K_D)s^2 + 281.6K_P s + 281.6K_I)} \tag{4.79}$$

$$G_{CL} = \frac{281.6\,(K_D s^2 + K_P s + K_I)}{s^3 + \frac{(1+281.6\,K_D)}{0.02092}s^2 + \frac{281.6K_P}{0.02092}s + \frac{281.6K_I}{0.02092}} \tag{4.80}$$

For the same denominator with equation 4.62, PID coefficients (K_D,K_P,K_I) are calculated as:

$$K_D = 0.0321 \tag{4.81}$$

$$K_P = 7.3547 \tag{4.82}$$

$$K_I = 601.7472 \tag{4.83}$$

$$C_{PID} = \frac{0.0321s^2 + 7.3547s + 601.7472}{s} \tag{4.84}$$

The controller is implemented in the real-time system. The continuous controller is converted to a discrete controller. The Matlab command ‘c2d’ is used with the option ‘tustin’ because the numerator order is higher than the denominator order. The Matlab code could be seen in Appendix Figure A.1. The discrete controller is:

$$C_{DISCRETE\_PID} = \frac{71.87z^2 - 127.8z + 57.16}{z^2 - 1} \tag{4.85}$$

CHAPTER 5

REAL TIME EXPERIMENTS

In order to see the performance of the designed controllers, they must be tested in a real-time system. Matlab and real-time platform xPC Target are tools for these tests. The system contains two computers, a data acquisition card, an I/O card, a servo amplifier, a power supply, and the fin actuation system (Figure 5.1). To implement load on the system there is an angular spring and a torque sensor. The spring applies torque when the fin turns. The spring constant is 5 Nm/degree and it has a linear behavior between ± 40 degrees. If the fin actuation system turns 12 degrees, there are 60 Nm load on the system (Figure 5.2).

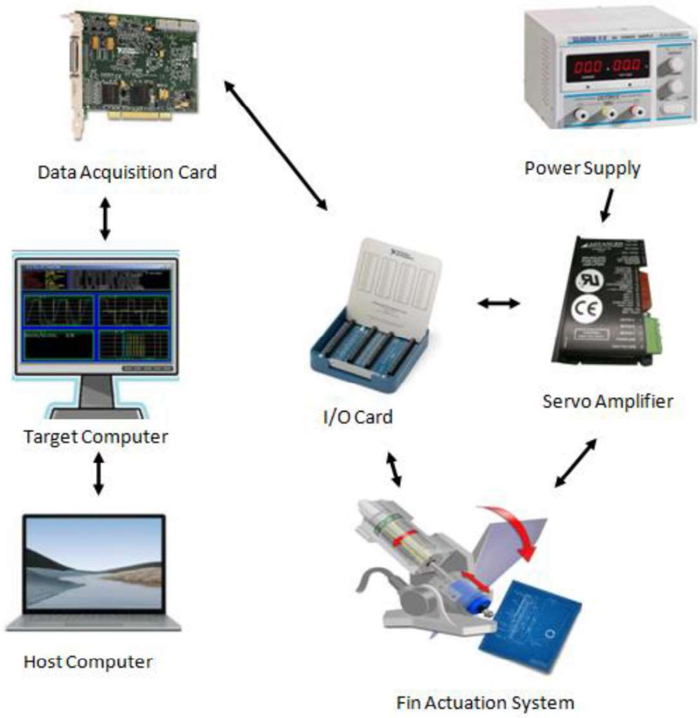

Figure 5.1 Real time test setup

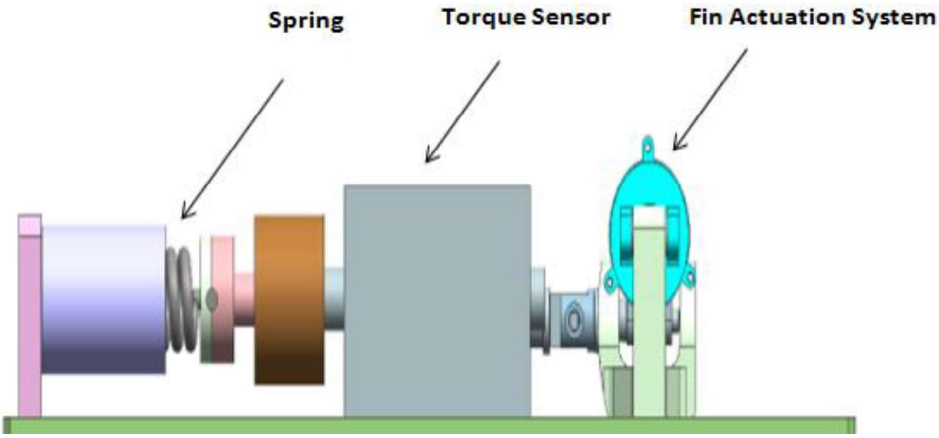

Figure 5.2 Fin load system [23]

5.1 Comparison of PID and State Feedback Controllers

State feedback controller with integral action and PID controller are designed and they have to be tested in a real-time system. After a controller comparison, which has better results could be used as the main controller. The reference which is given to the real-time system contains signals in step and sinusoidal form. The reference signal is limited with a rate limiter block. Because references in step form are not realistic and velocity of the rising interval is infinite. The rate limit value of the reference signal is ±300°/sec. This limiter can be seen in Figure 5.3. For these tests, no disturbance load was applied to the system.

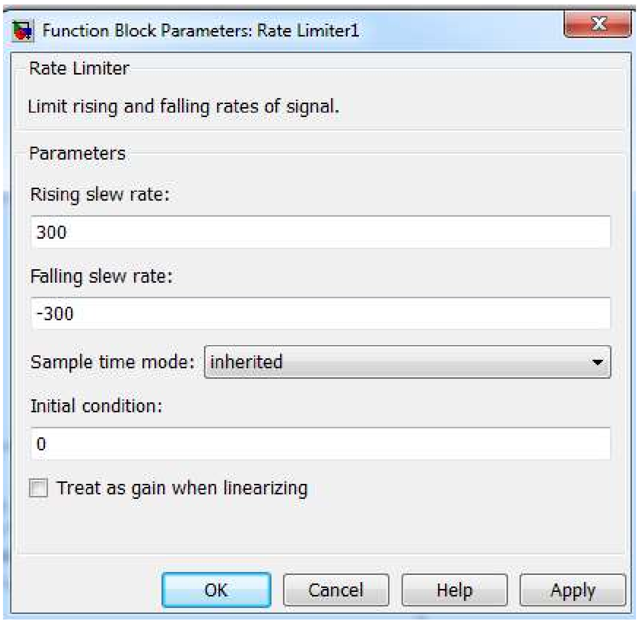

Figure 5.3 Rate limiter of the system

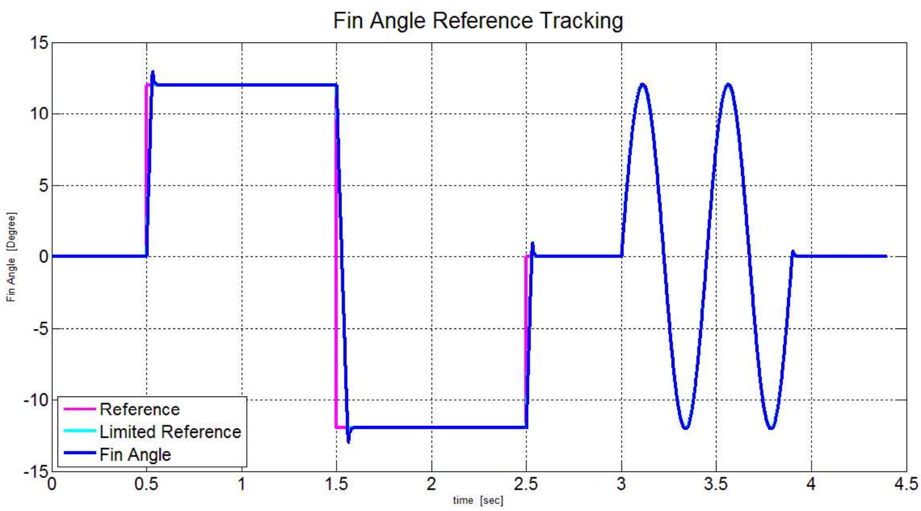

Figure 5.4 Response of PID controller

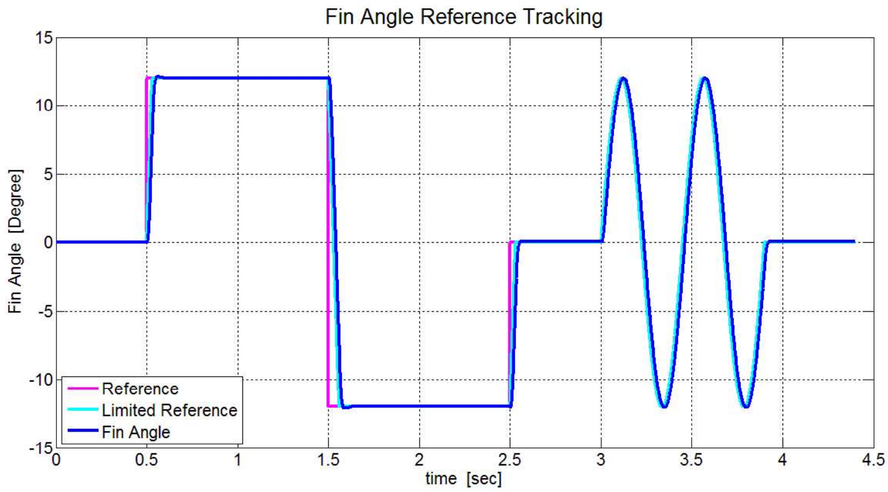

Figure 5.5 Response of state feedback controller

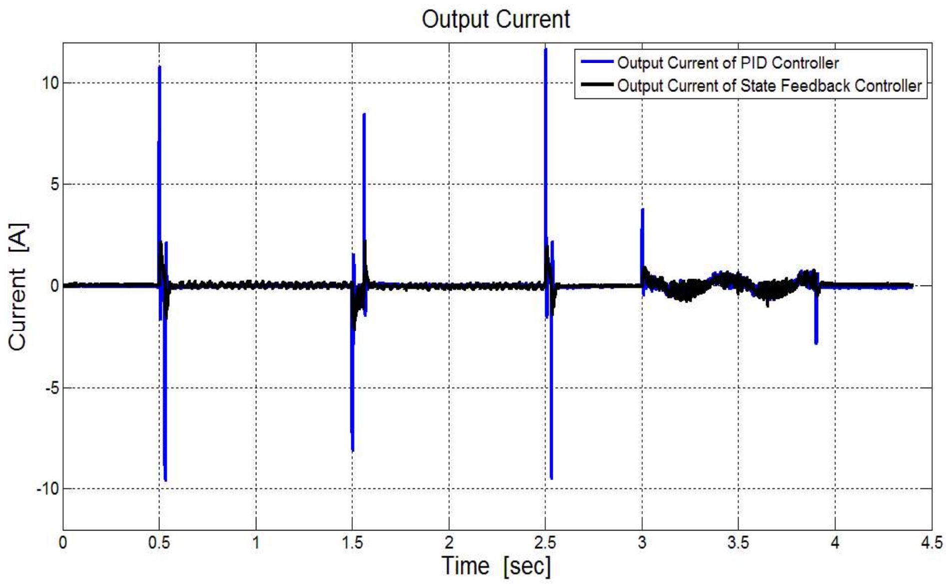

Figure 5.6 Current output of servo amplifier of PID and state feedback controllers

Table 5.1 Comparison of controllers

Controller	Settling time(%1)	Overshoot(12°)	Peak Current	RMS Current
PID	0.05 sec	% 8.3	11.65 A	0.5955 A
State Feedback	0.05 sec	< % 1	2.2 A	0.2557 A

Figure 5.4, Figure 5.5, Figure 5.6, illustrate the responses of two controllers and their required current. The settling times are similar. But PID controller has a higher overshoot and more current consumption. The Servo amplifier current output of the PID controller is more than five times higher than the servo amplifier current output of the state feedback controller (Table 5.1). State feedback controller is chosen, because battery capacity of missiles is limited. After these results, the state feedback controller was chosen as the main controller.

5.2 State Feedback Controller Real Time Test with External Load

While one encoder in the system measures the angle of rotation of the motor, the other encoder measures the fin angle (Figure 5.7). When the fin angle is obtained by using the encoder measuring the motor angle, the measurement is made more precise than the encoder that measures the fin angle directly. In other words it is as accurate as the transfer rate, assuming no backlash and deflection. Also, nonlinear phenomena due to backlash and deflection of mechanical components in the system have no effect on the designed linear controller. For this reason, the controller design was made with the system considered as linear.

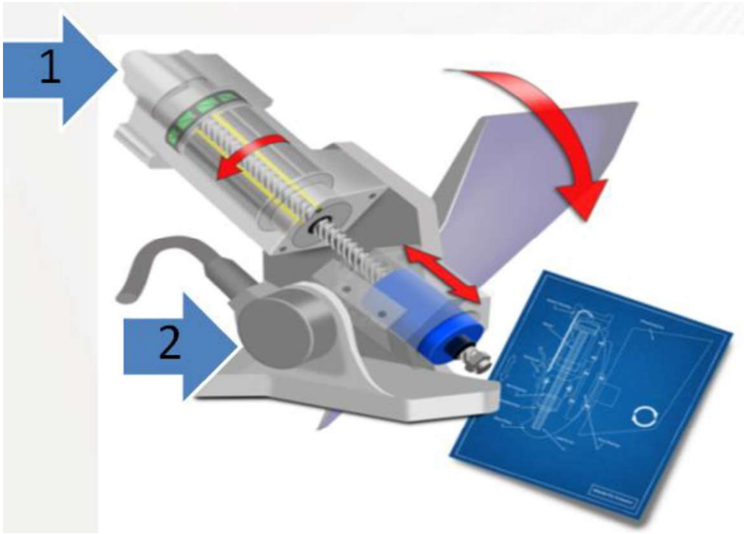

Figure 5.7 A fin actuation system with two encoders[24]

The disadvantage of obtaining fin angle by measuring from the motor side is that there are errors as much as backlash in mechanism and deflection of mechanical components in the system. The difference between the motor side encoder and the fin angle encoder when the fin angle reference which is 12 degree, is given to the system is shown in Figure 5.8.

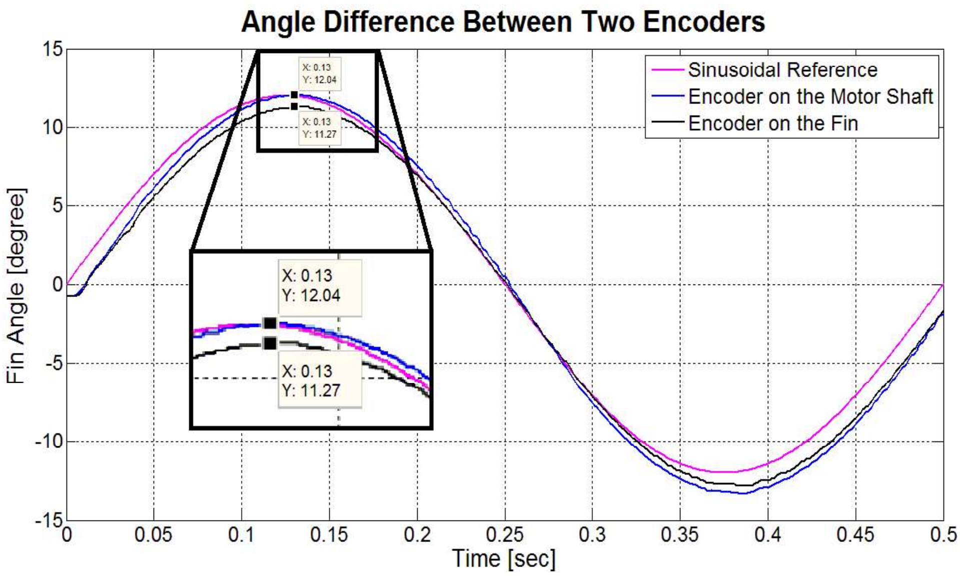

Figure 5.8 Angle difference between two encoders

Here, the fin angle obtained by deriving from the encoder measurement on the motor side against a 12-degree reference is 12.04 degrees, while 11.27 degrees is measured from the encoder on the fin side. That is, the controller which has only feedback from motor side, cannot detect the true angle value. For this situation, from fin side encoder is taken only measurement. In order to eliminate this situation, the controller feedback is added to the reference by subtracting the measurement difference of the two encoders from the measurement, which is taken from the motor side. This situation is shown schematically in Figure 5.9.

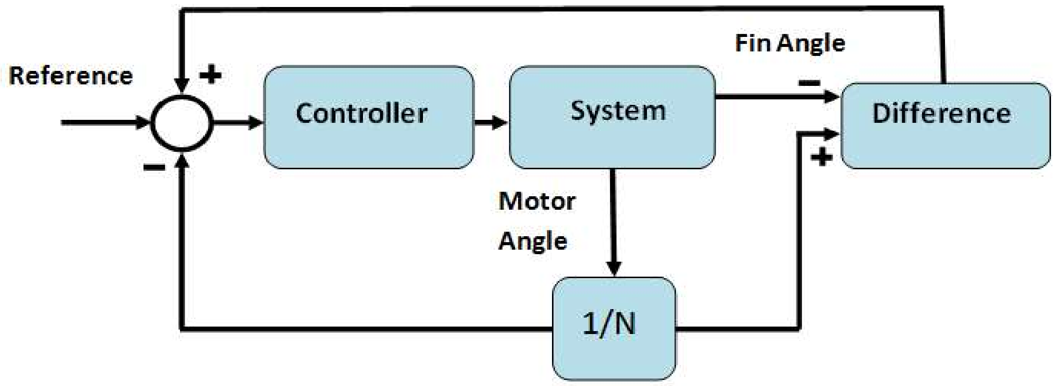

Figure 5.9 Angle difference compensation

The Simulink block configuration of this method can be seen in Figure 5.10 and Figure 5.11. Note that in Figure 5.11 obtained backlash was used in Figure 5.10.

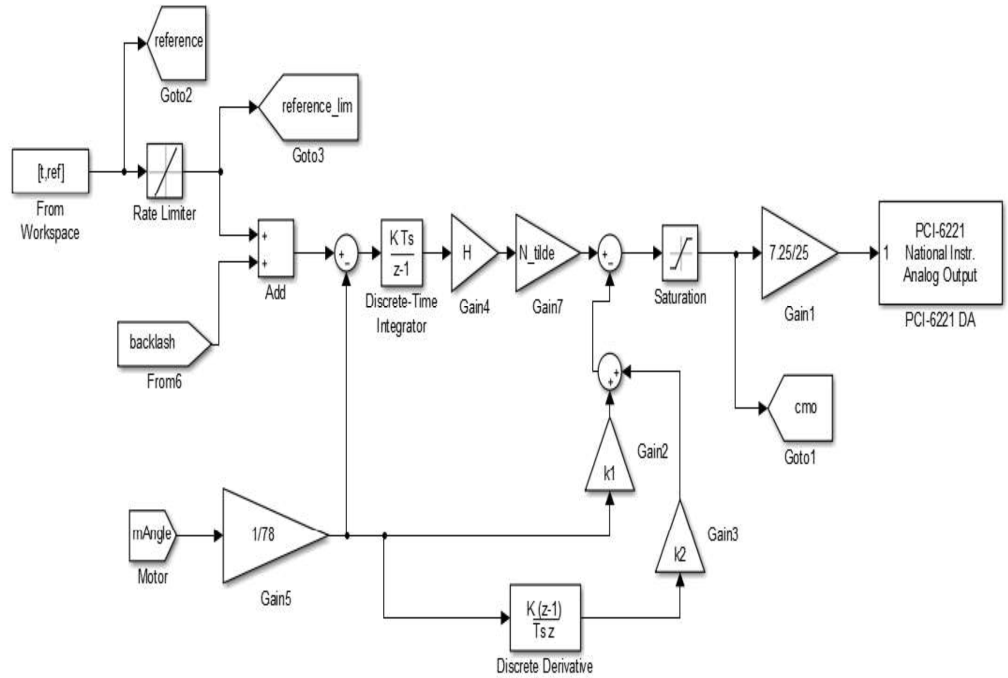

Figure 5.10 Simulink block diagram of state feedback controller with angle difference compensation

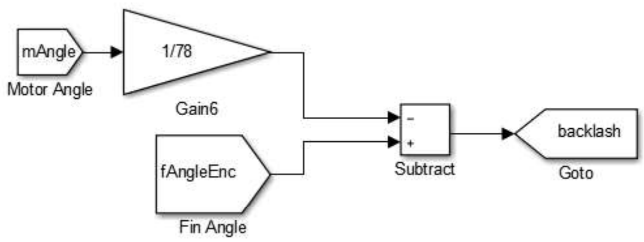

Figure 5.11 Backlash calculation block diagram

After the controller feedback of the system was adapted to the structure in Figure 5.10, the system was loaded with a Fin Load System, and tests were carried out. The load is applied to the system in inverse proportion to the fin angle with a spring in Fin Load System. The spring coefficient of the system, which is used in Fin Load System is about 5 Nm/degree and the applied load was measured with a torque sensor on the Fin Load System shaft. The reference, which was given to the system and the response of the system are shown in Figure 5.12, and the load on the system is shown in Figure 5.13. The augmented controller has no steady state error. And the fin angle follows the reference.

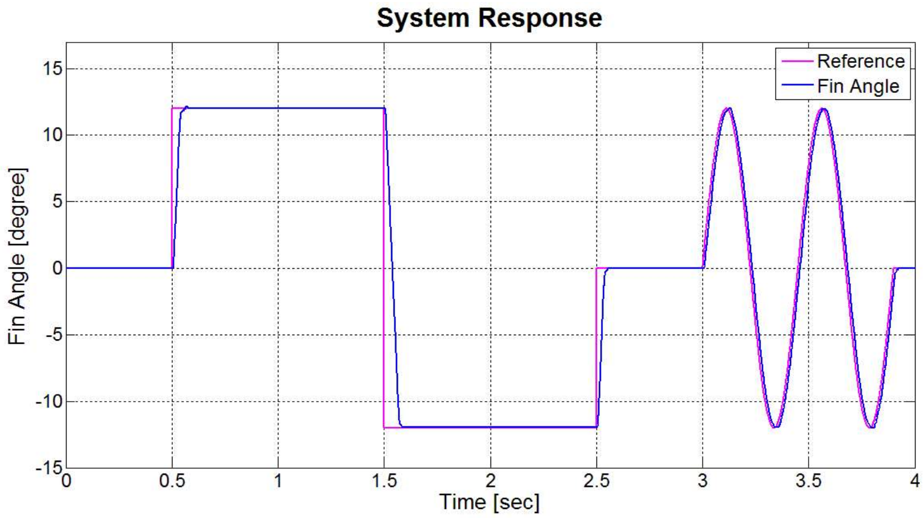

Figure 5.12 Reference response of controller

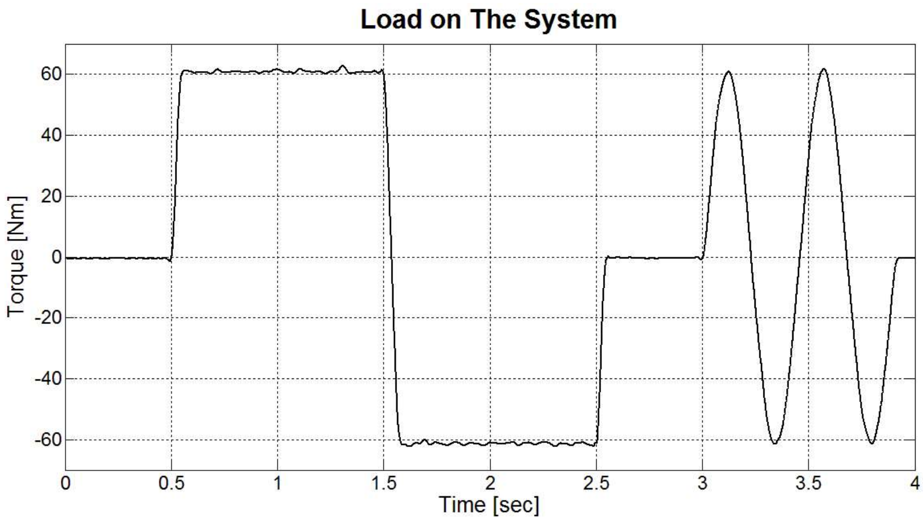

Figure 5.13 Load on the system

The current that the system consumes to achieve this performance is given in Figure 5.14. The RMS value of the current is 5.0903 A. It has an overshoot smaller than %1.

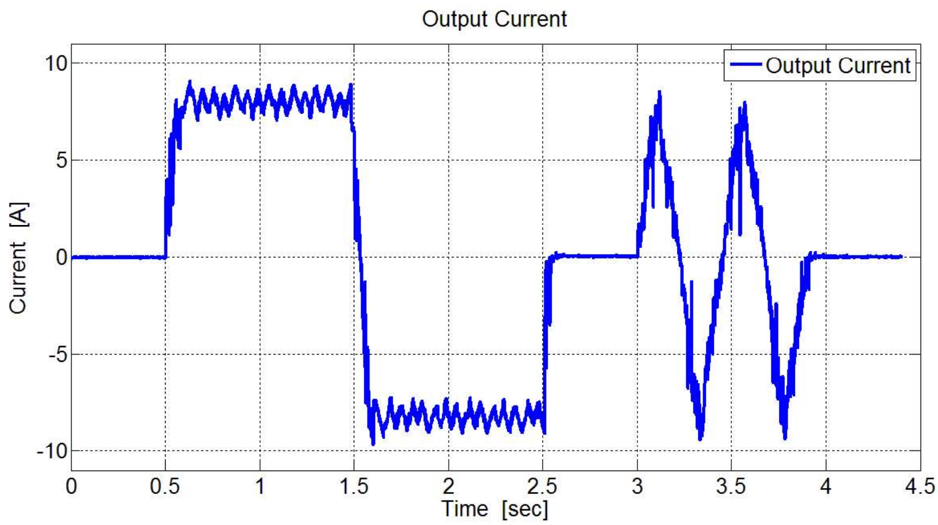

Figure 5.14 Output current of servo amplifier

CHAPTER 6

CONCLUSION

In this study, it is aimed to reduce the effects of the backlash caused by the mechanism and deflection in the control of the fin actuation system of the missile. In the first chapter, the literature was examined and an introduction to the study was given. In the second chapter, information about the system components and mechanism was given. In order to do this examination, sensors are placed in two separate locations of the mechanism. In the third chapter, system identification was explained with its theoretical background. In order to identify the system, data were collected by giving a current profile to the system. With these data, the mathematical model of the system was obtained by using the Box Jenkins noise model. With the system identification, the unknown parameters of the system, the viscous friction coefficient, and the moment of inertia of the system, were found. One of these parameters, the moment of inertia had been calculated using the kinetic energy formulation and it was shown that it is very close to the value founded by system identification. In the fourth chapter, controllers were designed and in the fifth chapter, the results of real-time tests were done. The first controller was designed with the state feedback method, and with a two-stage improvement, the controller was ensured not to make a steady-state error and to be resistant against disturbing effects. The second controller was designed as a PID with the same pole characteristic as the controller designed with the state feedback method. This controller was discretized to be used to compare two controllers. The model was tested in real-time with two separate controllers. The state feedback method controller, which was the controller that makes less overshoot and uses less power, was chosen. As a result of the tests carried out by applying the load with the loading system, the angle difference taken from the sensor on the motor side and the encoder measuring the fin angle was added to the reference and the controller was able to settle the correct angle. A non-linear system was controlled by a linear controller and the applied method. The test results were also graphically added to the study. As future work, new control studies can be done by using the hall sensor which is attached to the motor and an observer can be designed.

REFERENCES

[1] Zhou M., Mao D., Zhang M., Guo L. and Gong M., *"A Hybrid Control with PID–Improved Sliding Mode for Flat-Top of Missile Electromechanical Actuator Systems"*, Sensors , 18, 4449, 2018.

[2] Daş E., Delice I.I. and Keleş M. *"Analysis and robust position control of an electromechanical control actuation system"*, Transactions of the Institute of Measurement and Control, Vol. 42, No.3, pp. 628-640, 2018.

[3] Keleş, M. and Baykasoğlu C., *"Bir Kanatçık Tahrik Sistemi Yapısal Özelliklerinin Sistem Performansına Etkilerinin Sayısal ve Deneysel Olarak İncelenmesi"*, Gazi Journal of Engineering Science, Vol. 6, No.1, pp. 40-53,2020.

[4] Landau I. D., and Zito G.,*"Digital Control Systems: Design, Identification and Implementation "*, Springer-Verlag, London, 2006.

[5] Özbulur V., *"PID ve Kesir Mertebeli Kayan Kipli Kontrol Yöntemleri ile Doğru Akım Motorunun Hız Kontrolü"*, Afyon Kocatepe Üniversitesi Fen ve Mühendislik Bilimleri Dergisi, Vol. 17, pp. 537-545, 2017.

[6] Ramlı M. S., Rahmat M.F. and Najib M.S., "*Design and Modeling of Integral Control State-feedback Controller for Implementation on Servomotor Control*"6th Wseas International Conference on Circuits, Systems, Electronics, Control & Signal Processing, Cairo, pp. 208-213, 2007.

[7] *"Magnetic Encoders[online]"*, 1th ed., USA, Web address: https://www.dynapar.com/technology/encoder_basics/magnetic_encoder, [Accessed:26.12.2020].

[8] *"Brushless DC Motor Design[online]"*, 1th ed., Switzerland, Web address: https://www.portescap.com/en/products/brushless-dc-motors/bldc-motor-design, [Accessed:26.12.2020].

[9] Schröder D. *"Elektrische Antriebe- Grundlagen"*, 4th ed., Springer-Verlag, Berlin Heidelberg, 2009.

[10] Mehra R. K., Lainiotis D. G. *"System Identification Advances and Case Studies"*, Vol. 126, 1st ed., Academic Press, London, 1977.

[11] Aström K., Haeglund T., *"PID controller: theory, design, and tuning"*, ISA Society of America, Research Triangle Park,1994.

[12] S. S. Wilson,*"Understanding the PRBS signal as an optimum input signal in the wavelet-correlation method of system identification using multiresolution analysis",* Proceedings. IEEE SoutheastCon, Florida, pp.39-44, 2005.

[13] Peterson, W. and E. Weldon, Jr., *"Error-Correcting Codes"*,2nd ed., MIT Press, Cambridge, Massachusetts, 1972.

[14] Jammoussi H., Franchek M. A., Grigoriadis K., BooksM. *"Algorithm for closed loop system identification based on data correlation",* ASME Dynamic Systems and Control Conference, Michigan, pp. 433-438, 2008.

[15] Diversi R., Guidorzi R. and Soverini U., *"Identification of ARX models with noisy input and output"*, Proceedings of the European Control Conference, Greece, 2007.

[16] Diversi R., Guidorzi R. and Soverini U., *"Identification of ARMAX models with additive output noise"*, Proceedings of the 15th IFAC Symposium on System Identification, France, 2009.

[17] Maine R. E. and Iliff K. W., *"Application of Parameter Estimation to Aircraft Stability and Control: The Output-Error Approach"*, NASA Reference Publication 1168, USA, 1986.

[18] Ljung L. and Forssell U., *"Identification of Unstable Systems using Output Error and Box-Jenkins Model Structures"*,Proceedings of the 37th IEEE Conference on Decision and Control, Vol. 45, No:1, pp. 3932-3927, USA, 1998.

[19] Ljung, L., *"System Identification Toolbox™ R2014b",* Mathworks, 2014.

[20] Norlela I., Mazidah T., Hashimah I., Mohd H. F. R., Yahaya M. S., Ramli A. *"PID Studies on Position Tracking Control of an Electro-Hydraulic Actuator"*, International Journal of Control Science and Engineering,Vol.2,No.5, London, 2012.

[21] Paraskevopoulos, P. N., *"Modern Control Engineering"*, Marcel Dekker, Newyork, 2002

[22] Ogata K., *"Modern Control Engineering"*, Pearson, New Jersey, 2010.

[23] Cantürk, I., *"Güdümlü Bir Mühimmatın Elektromekanik Bir Bileşeni Olan Kanatçık Tahrik Sistemi İçin Gürbüz Kontrolcü Tasarımı Ve Uygulanması"*, Thesis (M.Sc), TOBB University, 2020.

[24] Nook C., *"Lead Screws Drive Missile Fin Actuation Systems [online]"*, 1th ed., USA, Web address: https://www.helixlinear.com/blog/lead-screws/lead-screws-drive-missile-fin-actuation-systems, [Accessed:26.12.2020]